

FACTORS INFLUENCING MATERIAL REMOVAL AND SURFACE FINISH OF
THE POLISHING OF SILICA GLASSES

by

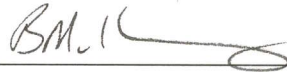
Alan Claude Landis

A thesis submitted to the faculty of
The University of North Carolina at Charlotte
in partial fulfillment of the requirements
for the degree of Master of Science in the
Department of Mechanical Engineering

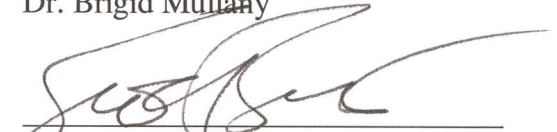
Charlotte

2006

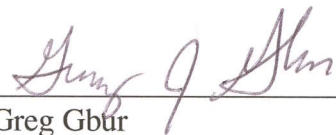
Approved by:



Dr. Brigid Mullany



Dr. Scott Smith



Dr. Greg Gbur

Report Documentation Page

Form Approved
OMB No. 0704-0188

Public reporting burden for the collection of information is estimated to average 1 hour per response, including the time for reviewing instructions, searching existing data sources, gathering and maintaining the data needed, and completing and reviewing the collection of information. Send comments regarding this burden estimate or any other aspect of this collection of information, including suggestions for reducing this burden, to Washington Headquarters Services, Directorate for Information Operations and Reports, 1215 Jefferson Davis Highway, Suite 1204, Arlington VA 22202-4302. Respondents should be aware that notwithstanding any other provision of law, no person shall be subject to a penalty for failing to comply with a collection of information if it does not display a currently valid OMB control number.

| | | | | | |
|--|------------------------------------|-------------------------------------|---|--|---------------------------------|
| 1. REPORT DATE 28 FEB 2007 | | 2. REPORT TYPE N/A | | 3. DATES COVERED | |
| 4. TITLE AND SUBTITLE Factors Influencing Material Removal And Surface Finish Of The Polishing Of Silica Glasses | | | | 5a. CONTRACT NUMBER | |
| | | | | 5b. GRANT NUMBER | |
| | | | | 5c. PROGRAM ELEMENT NUMBER | |
| 6. AUTHOR(S) | | | | 5d. PROJECT NUMBER | |
| | | | | 5e. TASK NUMBER | |
| | | | | 5f. WORK UNIT NUMBER | |
| 7. PERFORMING ORGANIZATION NAME(S) AND ADDRESS(ES) University of North Carolina at Charlotte | | | | 8. PERFORMING ORGANIZATION REPORT NUMBER | |
| 9. SPONSORING/MONITORING AGENCY NAME(S) AND ADDRESS(ES) | | | | 10. SPONSOR/MONITOR'S ACRONYM(S) | |
| | | | | 11. SPONSOR/MONITOR'S REPORT NUMBER(S) | |
| 12. DISTRIBUTION/AVAILABILITY STATEMENT Approved for public release, distribution unlimited. | | | | | |
| 13. SUPPLEMENTARY NOTES | | | | | |
| 14. ABSTRACT | | | | | |
| 15. SUBJECT TERMS | | | | | |
| 16. SECURITY CLASSIFICATION OF: | | | 17. LIMITATION OF ABSTRACT UU | 18. NUMBER OF PAGES 106 | 19a. NAME OF RESPONSIBLE PERSON |
| a. REPORT unclassified | b. ABSTRACT unclassified | c. THIS PAGE unclassified | | | |

The views expressed in this article are those of the author and do not reflect the official policy or position of the United States Air Force, Department of Defense, or the U.S. Government.

Alan Claude Landis

ABSTRACT

ALAN CLAUDE LANDIS. Factors influencing material removal and surface finish of the polishing of silica glasses. (Under the direction of DR. BRIGID MULLANY)

The polishing process is ancient form of material processing that has changed little in form over thousands of years. Even with all of the experience that the human race has gained on the subject, the underlying mechanism that promotes polishing still lies in the realm of theory. Of the existing theories available, each falls into one of two broad categories, chemical or mechanical removal mechanisms, or a combination of both. Effects of polishing pressure and velocity on material removal rate were analyzed. A novel method of controlling the polishing load will also be provided. Additionally, this work quantifies some of the factors that influence polishing, and then correlate the results to polishing theory. Specifically, abrasive polishing particle size and concentration, and abrasive polishing slurry pH were variables in a broad range of experiments, with other influencing factors kept as consistent as possible. The effects of pH were analyzed for interaction with the entire polishing system, as well as for effects on the polishing workpiece only. Silica materials were used as a baseline, and are polished on a synthetic optical polishing pitch with ceria (cerium oxide) abrasive particles. Finally, the experimental results will provide justification for a combined chemical-mechanical material removal model and form the basis of future work on more advanced materials like glass-ceramics and ultra low expansion glasses.

ACKNOWLEDGMENTS

Many people have provided support and guidance during the completion of this work. First, I would like to acknowledge the United States Air Force and the United States Air Force Academy for providing me the opportunity to extend my professional education. Dr. Brigid Mullany has provided exceptional guidance and stellar insight into this work, and has been the hand that shaped the final product and my growth as a student and researcher. I would like to thank the entire Mechanical Engineering Department at UNC-Charlotte for their support over my educational career, especially the support provided by Dr. Harish Cherukuri and Dr. Jerre Hill. Many thanks go to the dedicated professionals in the Center for Precision Metrology, most notably Roland Hege, for the willingness to share his vast knowledge in manufacturing. I would also like to thank Mr. Richard Speelman from Saint-Gobain Quartz for providing the raw fused silica materials free of charge, in the interest of supporting education and research. Lastly, I would like to thank Dr. Scott Smith and Dr. Greg Gbur for their participation by serving on the academic advisory board and for providing insightful directions to take the future work.

TABLE OF CONTENTS

| | |
|---|------|
| LIST OF TABLES | vii |
| LIST OF FIGURES | viii |
| LIST OF ABBREVIATIONS | xi |
| CHAPTER 1: INTRODUCTION | 1 |
| CHAPTER 2: BACKGROUND | 2 |
| 2.1 The Polishing Process | 3 |
| 2.1.1 Polishing Pitch | 4 |
| 2.1.2 Abrasive Slurry | 6 |
| 2.1.3 Workpiece Material | 8 |
| 2.2 Polishing Theories | 11 |
| 2.2.1 Mechanical Removal Theories | 12 |
| 2.2.2 Chemical Removal Theory | 15 |
| CHAPTER 3: THE CHEMICAL-MECHANICAL NATURE OF POLISHING | 17 |
| 3.1 The Chemical Tooth Model | 17 |
| 3.1.1 Effects of Water on Silica Materials and Polishing Agents | 18 |
| 3.1.2 Steps in the Chemical Tooth Model | 20 |
| 3.2 pH Effect on Colloidal Systems | 22 |
| 3.2.1 Influence of pH on Polishing Rates | 23 |
| 3.2.2 Surface Charge and Zeta Potential | 25 |
| 3.2.3 An Aside on Abrasive Slurry Dispersions | 26 |
| 3.3 Important Research Dealing with the Chemistry of Polishing | 28 |
| 3.4 Motivation for Current Work | 32 |
| CHAPTER 4: EXPERIMENTAL PROCEDURES | 34 |
| 4.1 Material Preparation | 34 |
| 4.1.1 Pitch Tooling | 35 |
| 4.1.2 Abrasive Slurry | 38 |
| 4.1.3 Workpiece Material | 39 |
| 4.2 Material Removal Rate Qualification Method | 40 |
| 4.2.1 Step Height Material Removal Rate Considerations | 40 |
| 4.2.2 Step Height Creation | 42 |

| | | |
|------------|---|----|
| 4.2.3 | Step Height Measurement Method | 44 |
| 4.2.4 | MRR Measurement Method Verification | 46 |
| 4.3 | Loading Conditions During Polishing | 47 |
| 4.3.1 | Pressure and Relative Velocity Experiments | 48 |
| 4.3.2 | Control Measures | 50 |
| 4.3.3 | Constant Load Device | 54 |
| 4.4 | Experimental Process | 55 |
| 4.5 | Measurement Methodology | 56 |
| 4.6 | Experimental Sets | 59 |
| 4.6.1 | Particle Size Effect Predictions | 59 |
| 4.6.2 | pH Effect Predictions | 60 |
| 4.6.3 | Slurry Density Effects | 61 |
| CHAPTER 5: | EXPERIMENTAL RESULTS | 62 |
| 5.1 | Particle Size Effect on MRR and Surface Finish | 62 |
| 5.1.1 | Material Removal Rate Results | 63 |
| 5.1.2 | Surface Finish Results | 65 |
| 5.2 | pH Effect on MRR and Surface Finish | 68 |
| 5.2.1 | Material Removal Rate Results with Anionic Dispersion | 68 |
| 5.2.2 | Surface Finish Results with Anionic Dispersion | 70 |
| 5.2.3 | Material Removal Rate Results with Non-Ionic Dispersion | 72 |
| 5.2.4 | Surface Finish Results with Non-Ionic Dispersions | 73 |
| 5.3 | Slurry Density Effect | 74 |
| 5.4 | Additional Comments on Experimental Results | 77 |
| CHAPTER 6: | DISCUSSION | 80 |
| 6.1 | Material Removal Theory | 80 |
| 6.1.1 | Mechanical Removal Theory | 80 |
| 6.1.2 | Chemical Removal Theory | 82 |
| 6.1.3 | Realities of Polishing | 84 |
| 6.2 | Slurry Dispersion Effects | 85 |
| CHAPTER 7: | CONCLUSIONS AND FUTURE WORK | 87 |
| REFERENCES | | 91 |

LIST OF TABLES

| | |
|---|----|
| TABLE 2.1: Parameters of the Nanophase Polishing Solutions | 8 |
| TABLE 2.2: Comparison of Crystalline Quartz and Fused Silica | 11 |
| TABLE 3.1: Comparison of experimental parameters, from [47] and [48] | 32 |
| TABLE 4.1: Mechanical Properties of Quartz and Zerodur [®] | 48 |
| TABLE 4.2: Results from variable load and lap velocity experiments | 49 |
| TABLE 4.3: Surface roughness measurement type characteristics | 58 |
| TABLE 5.1: Material removal rate effects of variable particle size | 63 |
| TABLE 5.2: Surface finish effects of variable particle size | 66 |
| TABLE 5.3: Material Removal Rate Effects of Variable pH (anionic dispersion) | 68 |
| TABLE 5.4: Surface Finish Effects of Variable pH (anionic dispersion) | 70 |
| TABLE 5.5: Material Removal Rate Effects of Variable pH (non-ionic dispersion) | 72 |
| TABLE 5.6: Surface finish effects of variable pH (non-ionic dispersion) | 73 |
| TABLE 5.7: Material Removal Rate Effects of Variable Slurry Density | 75 |
| TABLE 5.8: Theoretical calculations of variable density slurries | 77 |

LIST OF FIGURES

| | | |
|-------------|--|----|
| FIGURE 2.1: | Typical traditional polishing setup with a close-up of the polisher: (a) pitch type polisher and (b) pad type polisher | 4 |
| FIGURE 2.2: | Abrasive particles conforming to pitch under pressure | 5 |
| FIGURE 2.3: | TEM Micrograph of Nanophase Cerium Oxide Particles [9] | 7 |
| FIGURE 2.4: | 2-D representation of silica materials demonstrating (a) hexagonal crystalline structure and (b) amorphous structure | 9 |
| FIGURE 2.5: | Brown/Cook model of mechanical polishing: (a) plan view and (b) 3-d view | 14 |
| FIGURE 2.6: | Relationships between (a) polishing rate and glass acid resistance, (b) polishing rate and glass water resistance, and (c) polishing rate and micro-Vickers hardness of the glass surface [after 27] | 16 |
| FIGURE 3.1: | SiO ₂ and metal oxide surfaces exposed to H ₂ O | 18 |
| FIGURE 3.2: | Percent of silica surface Bronsted bases | 19 |
| FIGURE 3.3: | The chemical tooth model: (a) step 1 and (b) step 2 | 20 |
| FIGURE 3.4: | Possible fracture mechanisms for the chemical tooth model (Step 3) | 21 |
| FIGURE 3.5: | Steps 4 and 5 from the Chemical Tooth Model | 22 |
| FIGURE 3.6: | Theoretical surface charge dependence on pH for a metal oxide [after 37] | 23 |
| FIGURE 3.7: | MRR vs. pzc for various abrasive particles ([37], Fig. 1, p. G652, after [35]) | 24 |
| FIGURE 3.8: | Theoretical surface charge curves for various abrasive particles with differing pzc (system pH = 7) | 24 |
| FIGURE 3.9: | Solution particle acquired charges (after [42]) | 26 |
| FIGURE 4.1: | Major components of the Strasbaugh nFocus polishing apparatus | 34 |
| FIGURE 4.2: | Pitch tool pattern with cross-sectional cutaway | 36 |
| FIGURE 4.3: | Typical channeled pitch tool (12 inch diameter) | 37 |
| FIGURE 4.4: | Density and pH adjustment area | 39 |
| FIGURE 4.5: | Polisher interaction with recess: (a) pitch and (b) polishing pad | 41 |

| | |
|---|----|
| FIGURE 4.6: Photomicrographs of Recess Surface: (a) Initial and (b) after 2.554 μm removed | 41 |
| FIGURE 4.7: Recess surface lapped with (a) steel/opaline and (b) copper/diamond | 43 |
| FIGURE 4.8: Lapping tool mounted in zero-force chuck | 44 |
| FIGURE 4.9: Mask alignment to recess for step height measurement | 45 |
| FIGURE 4.10: Sequential Polishing Experiment Output ($\Delta = 188 \text{ nm}$) | 45 |
| FIGURE 4.11: Step height and mass removal rate method comparison | 47 |
| FIGURE 4.12: Polishing apparatus loading curve | 51 |
| FIGURE 4.13: Schematic of the load sensing device | 51 |
| FIGURE 4.14: Loading curves with (a) dead load on pad and (b) 10 psi overarm pressure on pad | 53 |
| FIGURE 4.15: Constant load application device | 55 |
| FIGURE 4.16: Polishing setup with recirculation system | 56 |
| FIGURE 5.1: MRR versus particle size for quartz and fused silica | 64 |
| FIGURE 5.2: Log-Log plot of MRR versus particle size | 65 |
| FIGURE 5.3: Comparison of surface finish measurements with (a) quartz and (b) fused silica, as a function of particle size. Polishing order (750 nm \rightarrow 40 nm \rightarrow 20 nm) | 67 |
| FIGURE 5.4: MRR versus pH for quartz and fused silica for anionic dispersion | 69 |
| FIGURE 5.5: Comparison of surface finish measurements with (a) quartz and (b) fused silica, as a function of pH (anionic dispersion). Polishing Order (pH 7 \rightarrow pH 10 \rightarrow pH 4) | 71 |
| FIGURE 5.6: MRR versus pH for fused silica with non-ionic dispersion | 72 |
| FIGURE 5.7: Comparison of surface finish measurements with fused silica as a function of pH with a non-ionic dispersion. Polishing Order (pH 7 \rightarrow pH 10 \rightarrow pH 4) | 73 |
| FIGURE 5.8: Comparison of fused silica surface from (a) anionic dispersion set ($R_a = 0.955 \text{ nm}$) and (b) non-ionic dispersion set ($R_a = 1.726$), both conducted at pH = 7 | 74 |
| FIGURE 5.9: Graphical representation of the variable density experiments | 75 |

| | |
|--|----|
| FIGURE 5.10: Representative 50X interferometer pictures of (a) fused silica (Ra = 0.600 nm) and (b) quartz (Ra = 0.296 nm). Both polished with 40 nm anionic dispersion at pH = 7 | 78 |
| FIGURE 6.1: Indentation of a sphere on a flat plate with (a) particle with a nominal load P and contact radius a and (b) particle with higher load P' and larger contact radius a' | 83 |
| FIGURE 6.2: Abrasive particle with polymeric coating interaction with silica | 85 |
| FIGURE 6.3: Comparison of pH experiments with anionic and non-ionic dispersion slurries | 86 |

LIST OF ABBREVIATIONS

| | | |
|---------------------|---|---|
| A | — | Area |
| a | — | Spherical Contact Radius (See Figure 2.5 and Figure 6.1) |
| AFM | — | Atomic Force Microscope |
| A_s | — | Mechanical Trough Area (See Figure 2.5) |
| Ce | — | Cerium |
| CeO_2 | — | Ceria (Cerium Dioxide) |
| C_p | — | Preston's Coefficient (cm^2/dyn) |
| CMM | — | Coordinate Measuring Machine |
| CMP | — | Chemical Mechanical Planarization |
| $\Delta H/\Delta t$ | — | Material Removal Rate (Change in thickness over time) |
| $\Delta s/\Delta t$ | — | Relative Velocity of Workpiece and Polisher |
| DI Water | — | De-Ionized Water |
| D_o | — | Mean Abrasive Particle Diameter (See Equation 2.3) |
| E | — | Modulus of Elasticity |
| FOV | — | Field of View |
| gm_f | — | grams force |
| GPa | — | gigapascals |
| h | — | Particle Penetration Depth (See Figure 2.5) |
| H^+ | — | Hydrogen Ion |
| H_2O | — | Water |
| H_3O^+ | — | Hydronium |
| HDPE | — | High Density Polyethylene |
| HNO_3 | — | Nitric Acid |
| iep | — | Isoelectric Point (pH level where zeta potential is zero) |
| k | — | Abrasive Particle Concentration (See Equation 2.3) |
| kg | — | kilogram |
| kPa | — | kilopascals |
| L | — | Load |
| lb_f | — | pounds force |
| mL | — | milliliters |
| mm | — | millimeter |
| MRR | — | Material Removal Rate |
| n_b | — | Percentage of Bronsted Bases on a Silica Surface |
| NaOH | — | Sodium Hydroxide |
| NIST | — | National Institute of Standards and Technology |
| nm | — | nanometer |
| O | — | Oxygen |
| OH^- | — | Hydroxide Ion |
| ρ | — | density |
| P | — | Pressure |
| pH | — | Potential of Hydrogen |
| psi | — | pounds force per square inch |

| | | |
|---------------------|---|---|
| pzc | — | Point of Zero Charge (pH level where particle surface charge = 0) |
| R | — | Radius of a Sphere (See Figure 2.5) |
| R _a | — | Arithmetic Average Surface Roughness |
| R _q | — | Root-Mean-Square Surface Roughness |
| R _{sk} | — | Statistical Skewness Value of a Line Profile |
| s | — | second |
| Si | — | Silicon |
| SiO ₂ | — | Silica (Silicon Dioxide) |
| SiOH | — | Silanol Group |
| Si(OH) ₄ | — | Silicic Acid |
| μm | — | micrometer |

CHAPTER 1: INTRODUCTION

The polishing process is sometimes referred to as an art form, rather than a strict scientific discipline. Part of this misnomer lies in part to the often encountered inability to get repeatable and accurate results. This inability to predict outcomes stems from the fact that there is no one set theory that can describe the polishing process. This thesis will offer supporting evidence to one or more of the competing theories in polishing.

Of the different theories available, the experiments presented herein will address two broad categories, chemical and mechanical removal mechanisms. Specifically, the influence of polishing slurry pH and abrasive particle size and concentration on material removal rates (MRR) and surface finish will be investigated and analyzed with respect to the existing theories. It is important to attempt to understand these mechanisms because an understanding leads to process improvement. Polishing is one of the most expensive machining processes, in terms time and labor costs. Depending on the required surface finish, optic size, and amount of surface roughness from preceding machining operations, a material could remain on the polishing system for hours to days.

For most optical manufacturers, polishing is the only available method to achieve nanometer and sub-nanometer surface finish and will likely remain an integral process step for many years. Thus, attempting to understand the underlying mechanisms and basic science associated with the polishing process is crucial to, in turn, develop methods and procedures to reduce cost, trim schedule, and bolster performance.

CHAPTER 2: BACKGROUND

For many years, researchers have attempted to predict the underlying mechanism responsible for the polishing of glass, metals, and composites. Before any attempt to understand the polishing process, a brief introduction to the history is essential. The ability to polish objects, regardless of intended purpose, has existed for thousands of years. In ancient times, the ‘shiny’ surfaces generated from polishing were most assuredly more decorative than functional for these early civilizations. Lu, et al [1], examined highly polished corundum axe fragments found at an ancient Chinese settlement at Zhejiang Yuhang Wujiabu, circa 2500 BC. They found through Atomic Force Microscopy (AFM) that the surface roughness was on the order of a few nanometers. This is a humbling fact, considering that over the past 4500 years, humankind has only increased in polishing ability on the order of several nanometers.

As the human race developed, surface quality transformed from decorative to an essential function for certain applications, namely the telescope. In the 17th century, scientists like Galileo began to contribute to the body of astronomical discoveries. Researches like Miniati, et al [2], have used modern measurement techniques to study lenses of this era and found that they were of superb quality for the time, having only minor features present on the polished surfaces.

2.1 The Polishing Process

Many different types of polishing exist, including chemical mechanical planarization (CMP) used in integrated circuit chip manufacturing, float polishing, magneto-rheological finishing (MRF), and traditional polishing. Traditional polishing can be further sub-divided into sub-aperture polishing where the workpiece is larger than the polisher, and full aperture polishing where the workpiece is smaller than the polisher. The current work utilizes full aperture traditional polishing.

The polishing process can be thought of as a wear mechanism between the workpiece being polished and the abrasive particles held by a medium. The abrasive particles are usually in a liquid mixture, known as slurry. Material removal occurs from the workpiece-particle interaction through a mechanical or chemical mechanism, or a combination of both. The polishing medium is typically a material such as pitch (a highly viscous fluid) or a polishing pad. The system made from the combination of the polishing medium and abrasive particles is often referred to as a polisher.

Traditional polishing is performed by placing the workpiece in contact with the polisher, under pressure, and developing a relative velocity by rotating the polisher and translating the workpiece. With pitch, slurry application allows the abrasive particles to become embedded under the applied pressure and protrude out to promote wear on the workpiece surface. With a pad type material, the fibrous structure (asperities) holds the abrasive particles against the workpiece surface, again promoting wear. Figure 2.1 shows the process with both pitch and pad type polishing.

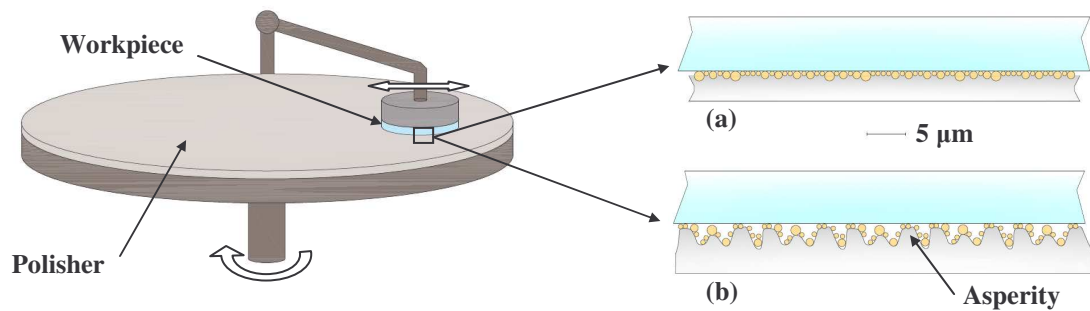


Figure 2.1: Typical traditional polishing setup with a close-up of the polisher: (a) pitch type polisher and (b) pad type polisher

2.1.1 Polishing Pitch

Optical polishing pitch was the chosen material for the majority of the experiments contained in this thesis. Pitch is a highly viscous material that can be manufactured from man-made or natural materials. The bulk majority of available pitch is manufactured from natural sources. Organic materials, such as coal, wood, rosin, and petroleum, when refined, produces the characteristic pitch used by opticians [3, 4]. Pitch has been in used for hundreds of years, with the recommendation of using wood based pitch dating back to Sir Isaac Newton [5].

Because pitch is a very viscous fluid, it can be thought of in terms of a self-regulating system. When abrasive particles are introduced to pitch under polishing conditions, the larger particles will bear more load, and sink rapidly into the pitch surface. These large particles will sink until the smaller particles then come into contact. This process continues until all the particles share in support of the workpiece, shown schematically in Figure 2.2 [6].

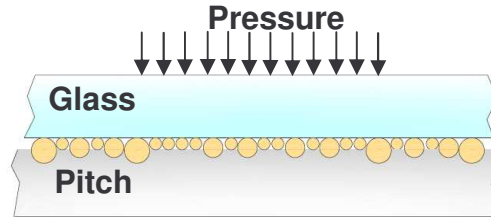


Figure 2.2: Abrasive particles conforming to pitch under pressure

For the current work, Acculap polishing pitch was obtained from Sutton Technologies, which is a synthetic polymer based material. Natural pitches can be subject to variations from batch to batch due to differences in the materials used in the manufacturing process and, since it is organic, can break down over time. Using a synthetic pitch, the properties should remain consistent between different laps. Acculap has a proprietary recipe, but the basic components are a poly(alpha-methyl)styrene polymer base, with hydrogenated oil added to promote flow [7]. Variable amounts of these products, along with other additives, create grades of pitch with differing hardness and viscosity. Those familiar with polishing would benefit from knowing that the synthetic pitches have been shown to perform similar to traditional pitches of the same viscosity. The 'Standard' grade Acculap, with a shear viscosity of 0.467 GPa-s, was used for the production of the pitch tools in this thesis, and comparable to the commonly used traditional pitch, Gugolz 64, which has a measured shear viscosity of 0.393 GPa-s [7].

Pitch is typically applied to polishing platens by pouring hot pitch onto the platen surface and allowed to cool. After the cool-down period, grooves are cut into the pitch surface to promote slurry flow to the workpiece. This allows the introduction of new polishing particles and also carries away any material that has been removed from the workpiece surface. Various properties of laps (channel configuration, lap depth, channel

depth, hardness, etc.) have been studied and shown to influence the overall form and surface finish of the workpiece [3, 4, 5, 8]. However, the configuration of the lap is not considered a variable in the current work, so baseline materials and patterns were chosen and kept constant throughout.

2.1.2 Abrasive Slurry

Polishing slurries are mixtures of abrasive particles and a suspension medium which, in polishing, is almost exclusively water. The liquid phase of the mixture allows the particles to flow under the workpiece for interaction. There are many different types of abrasive particles available, but the most common ones used are diamond, silica (SiO_2), and several metal oxides, namely, ceria (CeO_2) and alumina (Al_2O_3).

Abrasive particles for slurries can be obtained in several forms. One of the most common is raw abrasive in powder form. These powders are typically high purity abrasives. The slurries are prepared by simply mixing the powder in water, controlled by adding a certain mass of abrasive to a measured volume of water to obtain the desired density for the polishing application.

The other supplied form is in colloidal solution. A colloidal solution is one that consists of one material phase (i.e. solid, liquid, gas) existing in another. In the case of polishing slurry, the system is a solid (abrasive particle) dispersed in a liquid (polishing dispersion). These solutions are supplied with a known weight percent of abrasive, which can be diluted with water to obtain the desired density. An important note on colloidal polishing solutions is that the dispersion may contain other additives, which are brand specific to the manufacturer, and may or may not be known.

The abrasive particles used for this thesis were colloidal ceria solutions obtained from Nanophase Technologies. The cerium oxide particles contained in these solutions are nanocrystalline and of high purity, created using a patented plasma arc process that ensures uniform particle size [9]. A TEM micrograph of typical Nanophase produced ceria particles are shown in Figure 2.3. The ceria dispersion recipe is proprietary, but is known to be water based.

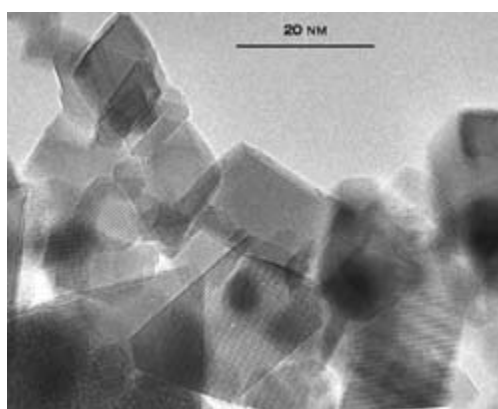


Figure 2.3: TEM Micrograph of Nanophase Cerium Oxide Particles [9]

Four different particle dispersions were used in the main polishing experiments. These are summarized in Table 2.1. As seen, the first three differ only in particle size, with the exception of the composition of the CE-6080 dispersion, which contains a small amount of glycerin to prevent sticking when polishing glass on pitch. Each of these slurries also contains an amount of added polymers to aid in stabilization of the solutions. The added polymers have an associated negative charge, thus their distinction in the table as anionic. The fourth type, CE-6086, contains particles that also have a polymeric coating, but these polymers have no associated charge. The distinction between the two dispersions is the method to prevent agglomeration of the particles [10, 11, 12]. This will be discussed in further detail, but some background is needed first. For now, it is only

important to remember that the fourth particle dispersion (CE-6086) is fundamentally different than the first three.

Table 2.1: Parameters of the Nanophase Polishing Solutions

| Product Name | Mean Particle Diameter (nm) | Dispersion | Out of Box pH | Recommended pH Usage Range |
|---------------------|------------------------------------|-------------------|----------------------|-----------------------------------|
| CE-6080 | 750 | anionic | ~ 8 | 7-12 |
| CE-6082 | 40 | anionic | ~ 8 | 7-12 |
| GP-18HD | 20 | anionic | ~ 8 | 7-12 |
| CE-6086 | 40 | non-ionic | ~ 8 | 4-11 |

2.1.3 Workpiece Material

Many different types of materials may be polished including metals, ceramics, glass-ceramics, and glass. Copper and silicon polishing has been of key interest over the last twenty years due to the necessity of the polishing process in the manufacture of integrated circuit chips. The majority of polishing, however, still lies in the realm of glass and glass-ceramic substrates which are used in a vast amount of applications, from optics for lithographic machines to mirrors and lenses for laser systems.

Before discussing the baseline materials used in the research, it is important to provide a distinction between glasses and crystalline materials. When the term glass is used, solid objects such as window panes and car windshields come to mind. However, glass is not technically a solid. Glasses exhibits properties of supercooled liquids, that is, when cooled past the melting point, they continue to be cooled in the liquid state. Thus, it does not crystallize, and forms a material with no long range crystalline order. Glasses are generally considered supercooled, highly viscous liquids, better known as an

amorphous or vitreous material. These are different from crystalline materials that have fixed interatomic bonding angles, having a repeating geometric form [13].

The body of work contained in this thesis focuses on silicon dioxide (silica) materials, namely, crystalline and vitreous silica. Both have the exact same chemical composition, (SiO_2), but are fundamentally different materials. From the definitions in the previous paragraph, the obvious difference between the two is that crystalline silica exhibits atomic ordering and the vitreous silica does not, putting it in the category of glass. The atoms of both are in a tetrahedral arrangement with each silicon atom surrounded by four oxygen atoms, with the oxygen atoms being shared between tetrahedra. Figure 2.4 represents both forms in 2 dimensions [14].

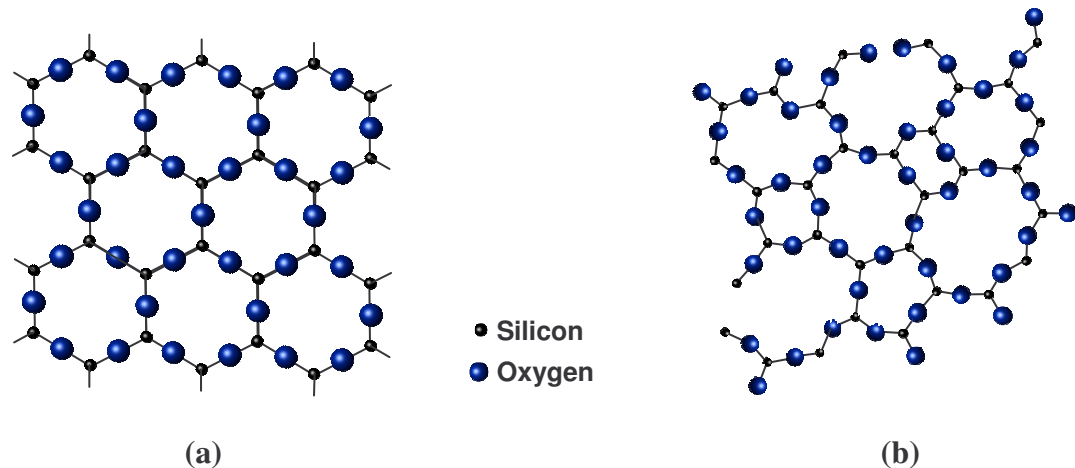


Figure 2.4: 2-D representation of silica materials demonstrating (a) hexagonal crystalline structure and (b) amorphous structure

Quartz

The basic form of crystalline silica is quartz and its polymorphs (e.g. coesite, cristobalite, stishovite, and tridymite) and is optically uni-axial along the z-axis (growth axis) [15]. The silica tetrahedrons are arranged in a spiral structure along the z-axis in

either a right or left screw orientation, which equates to polarizing transmitted light either right or left, with the amount of rotation as a function of the material thickness and wavelength of the propagating light [16].

The quartz used for experimentation was procured from Sawyer Technical Materials, LLC and was laser grade with the optical axis (z-axis) perpendicular to the polishing surface. Quartz is the most abundant mineral in the earth's crust [15], but natural crystals seldom meet the specifications for today's market, generating the need for man-made materials. Sawyer produces the quartz hydrothermally, by growing the single crystal in an autoclave. The growth is typically in the z-direction, and the bars are lumbered to generate the appropriate crystal orientation blanks, although the growth can be in other directions dependent upon the seed crystal [17]. Quartz, like metals, can exist in different phases. Although not specifically stated by the manufacturer, the material was determined to be β -quartz, based on comparing the supplied and measured density with that in literature [18]. Quartz use is found in a wide range of applications including inclusion in electronic devices (due to exhibited piezoelectric properties) and in optical and laser applications.

Fused Silica

The fused silica glass used for experimentation was Spectrosil[®] 2000 laser grade material from Saint-Gobain Quartz. The fused silica is manufactured by a chemical vapor deposition process, generating a high purity (99.9999% SiO₂), deep ultra-violet optical grade glass that is fluorescence and bubble free. Fused silica is used in an extremely wide array of applications including lithography optical systems, laser optics,

and optical components in deep ultra-violet, visible, and near infra-red systems [19, 20]. A comparison of the two materials is provided in Table 2.2.

Table 2.2: Comparison of Crystalline Quartz and Fused Silica

| | Quartz | Fused Silica | Units |
|--|-------------------------------------|--------------|------------------------|
| Density ^{a,b} | 2.65 | 2.21 | g/cm ³ |
| Young's Modulus ^{a,b} | 103 ⁼ (78 [⊥]) | 74 | Gpa |
| Hardness ^{a,c} | 7 | 7 | Mohs |
| Poisson's Ratio ^{d,c} | 0.056 | 0.17 | |
| Coef. of Thermal Expansion ^{e,f} | 9.91 | 0.54 | x10 ⁻⁶ / °C |
| Crystal System ^g | Hexagonal | - | |
| Class ^g | 32 | - | |
| Lattice Constants ^g | a = 4.9133 c = 5.4053 | - | Å Å |

a - Ref [21], b - Ref [22], c - Ref [19]

d - Calculated from theoretical equation provided by [23] using [21] data

e - Average calculated from [saywer] data in the range 0 - 573 °C

f - Average value 0 - 1000 °C, provided from [22]

g - Ref [15]

= - Parallel to the z-axis ⊥ - Perpendicular to the z-axis

2.2 Polishing Theories

Since the time of Newton, polishing has been thought of as a wear process between workpiece material and abrasive particle interactions. However, the underlying mechanics were still not understood. Several theories have emerged to attempt to explain the intricacies involved, and can be generally lumped into two broad categories, mechanical removal theories and chemical removal theories. Evans, et al [25], provides an excellent summary of all of the prevalent removal theories available. A key point to understand before reviewing these theories is that none of them fully explain every aspect of polishing.

2.2.1 Mechanical Removal Theories

Several different models will be discussed under this category. They are all based on the mechanical removal of material through interaction of the abrasive particles with the workpiece, and the subsequent scratching/fracturing of the polishing surface.

Rayleigh and Beilby

Two of the major theories in polishing in the early 20th century were proposed by Lord Rayleigh and Sir Beilby. Rayleigh's theory suspected that abrasive particles pressed against the glass surface and created mechanically fractured sites. The material at these sites was then removed on a very small scale (molecular level) [26, 27]. Beilby, conversely, proposed a theory that the material 'flowed' under interaction with the abrasive particles. It was thought that the glass was locally heated by frictional interaction with the abrasive particle, creating a less viscous material at the surface. This 'flowed' layer could then either be removed by the traversing particles, or allowed to flow over the surface. This notion of 'flow' was reasoned to be the process of obtaining a very smooth finish on glass. [27, 28].

Preston

The work of Preston in 1927 [29, 30] led to the development of a model to predict removal rates by controlling several factors, including an empirically derived coefficient based on particular polishing materials and conditions. Equation 2.1 shows the formula, with $\Delta H/\Delta t$ the change in material thickness over time, L is the load, A is the effective polishing area of the workpiece, $\Delta s/\Delta t$ is the relative velocity between the workpiece and

lap, and C_p is a material/lap specific coefficient. The later value would eventually bear his name, the Preston's coefficient, which is a parameter still in use today.

$$\frac{\Delta H}{\Delta t} = C_p \cdot \frac{L}{A} \cdot \frac{\Delta s}{\Delta t} \quad (2.1)$$

Brown and Cook

The Preston model existed unchallenged for many years until the work of Brown, et al [31, 32], which focused on the optical polishing of metals. It was surmised, through mathematical modeling and experimentation, that the removal rate equation varied with the inverse of Young's Modulus of the material being polished. The model was based on spherical particles elastically indenting the metal surface, governed by Hertzian indentation, and then gouging a path through the material. The model developed is given in Equation 2.2, with L/A being replaced by pressure (P) and C_p replaced by the inverse of twice Young's Modulus. Brown and Cook [33] later suggested that the model could also describe glass polishing, under certain conditions.

$$\frac{\Delta H}{\Delta t} = \frac{P}{2E} \cdot \frac{\Delta s}{\Delta t} \quad (2.2)$$

Figure 2.5 shows a plan view of the proposed contact mechanism. 'R' is the radius of the penetrating sphere, 'h' is the penetration depth, and 'a' is the radius of the indentation contact area. A_s is the 'gouge' surface area, shown as the purple area below the dashed line in Figure 2.5(a) and also shown on the 3-d representation in Figure 2.5(b).

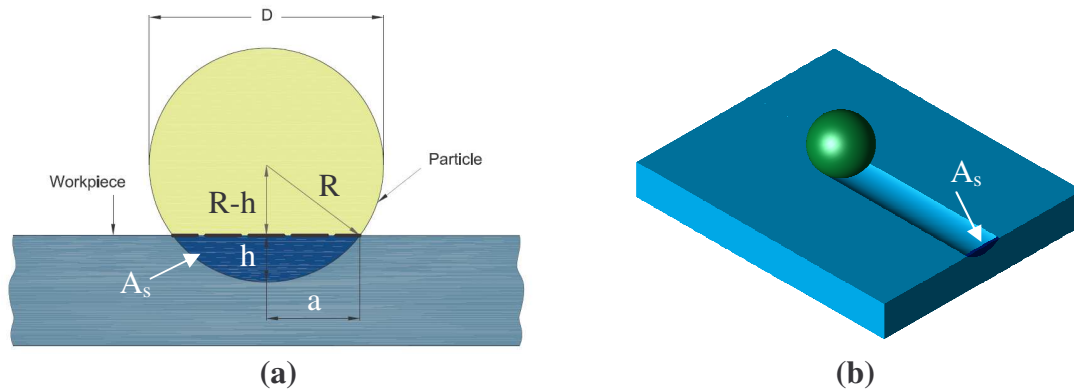


Figure 2.5: Brown/Cook model of mechanical polishing: (a) plan view and (b) 3-d view

An important note about this model is that abrasive size and concentration are not in the final form, even though they were used in the development of Equation 2.2, due to cancellation. The model thus states that the material removal is independent of abrasive size and concentration, with limits applied. According to Brown, the analysis is subject to ensuring that enough particles are available to support the load without indenting to a great depth, but still be few enough for the particles to act independently. He additionally notes that these conditions will remain for some broad range of conditions [34].

Another note is that even though the removal rate prediction did not rely on particle size and concentration, it was also shown that the predicted surface finish would be affected. Using the same basic hertzian mechanics, it was shown that roughness can be described by Equation 2.3:

$$R_s = \frac{3}{4} D_o \left(\frac{P}{2kE} \right)^{\frac{2}{3}} \quad (2.3)$$

where R_s is the roughness, D_o is the mean particle diameter, and k is particle concentration (unity for fully a fully filled volume) [34, 35]. This is attributed to the fact

that with smaller particles carrying the load (versus large particles), the resulting indentation depths will be less and reduce the surface roughness.

2.2.2 Chemical Removal Theory

The chemical theory, as described by Izumitani [27], is attributed to Preston and Grebenshchikov, and was a departure from the common thought on polishing. The chemical theory involves creation of a gel layer formed by silica glass in the presence of water. This layer could then be removed by interaction of the glass surface with the abrasive particles.

In this work, Izumitani tested the theories of mechanical and chemical removal by subjecting eighteen different optical glasses to conditions that were underlying in each theory. If the abrasive theory is correct, then the material removal rate should rely on strength of the glass. If flow theory is at play, then the rate should depend on the softening point of glass. The experiments found no correlation of the above, reasoning that neither of these hypotheses was correct [27].

It was also surmised that if there was a chemical aspect to polishing, then the polishing rate should be proportional to the chemical durability of the glass. Additional experiments were performed, measuring the polishing rate versus chemical durability characteristics (Figure 2.6 (a) and (b)) and the rate versus the micro-Vickers hardness of the polishing surface (Figure 2.6 (c)). Indeed, it was shown that the polishing rate is dependent upon how susceptible the glass is to water (formation of a hydrated layer) and the relative hardness of that layer [27]. Tomozawa [36] supports the results shown in Figure 2.6 (b). In words, the soft layer formed chemically on glass is removed by a mechanical action of the abrasive. While this work gives insight into the chemical

aspects, there was still a need to understand the conditions that controlled the chemical reactions, and will be the subject of Chapter 3.

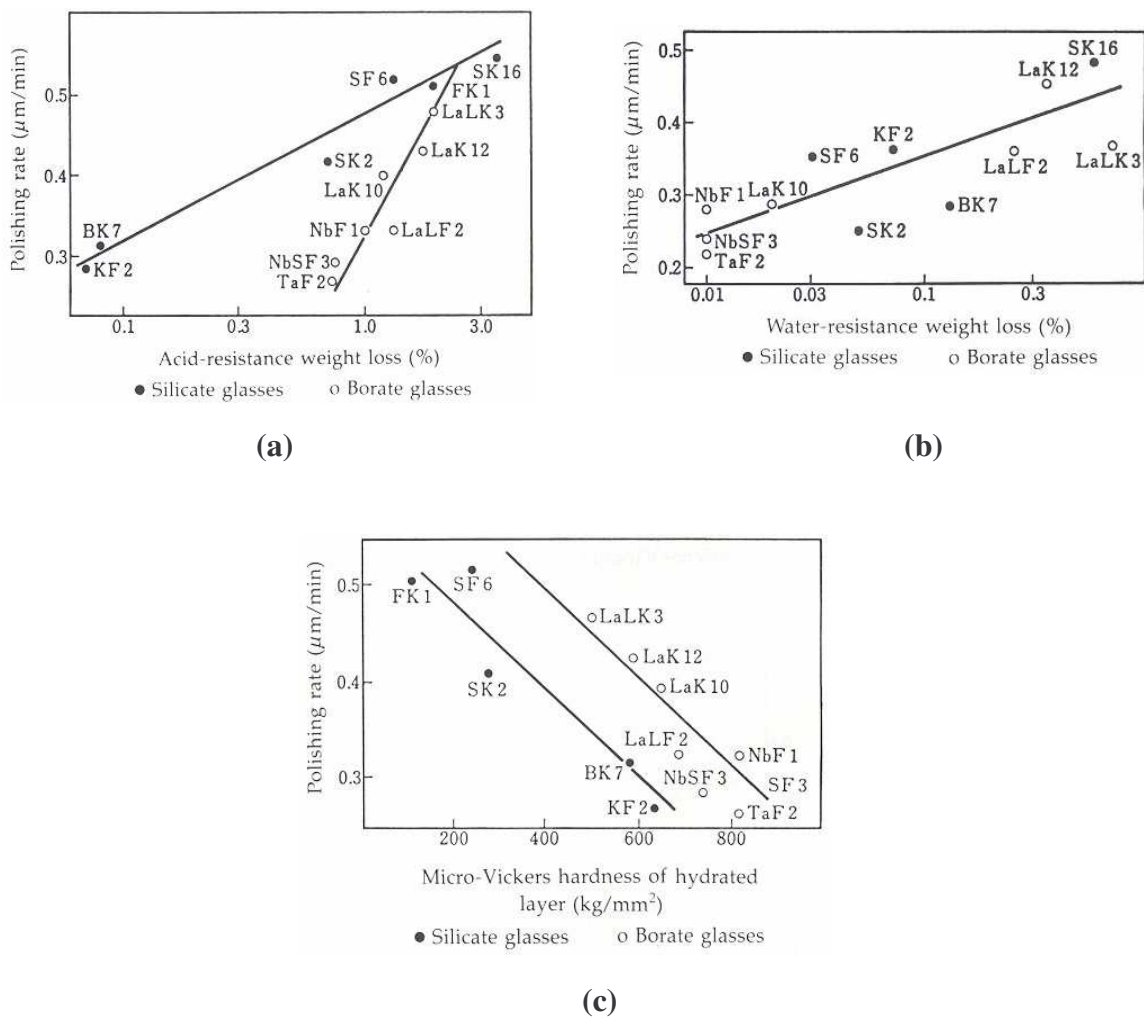


Figure 2.6: Relationships between (a) polishing rate and glass acid resistance, (b) polishing rate and glass water resistance, and (c) polishing rate and micro-Vickers hardness of the glass surface [after 27].

CHAPTER 3: THE CHEMICAL-MECHANICAL NATURE OF POLISHING

Of the theories described previously, it was noted that none of them fully explain every aspect of polishing. This, in turn, leads to an assumption that one or more of the theories are actually working together in a combined hypothesis. A major push utilizing this idea was by Cook [35] in the early 1990's, in which he studied the combined chemical-mechanical nature of polishing. This seminal paper on the subject provided a great deal of inspiration for research and discussion.

In the work, a material removal process is described that is governed by both mechanical and chemical interaction of the abrasive particles with the glass workpiece. This type of removal mechanism was termed the 'chemical tooth,' versus the 'mechanical tooth' indicative of an abrasive process. The bulk of the information in this chapter comes from Cook [35], Osseo-Asare [37], and Paul [38], but care has been taken to annotate the resource when specific information is supplied.

3.1 The Chemical Tooth Model

To explain the chemical tooth model, a particular interaction scheme will be used, namely, silica (SiO_2) glass polishing with metal oxide abrasive particles. This scheme will mirror the experimentation in this thesis, and hopefully provide a better understanding into goals of the research. A brief introduction to the importance that water plays in the chemical model will be given, followed by the main steps in the theory.

3.1.1 Effects of Water on Silica Materials and Polishing Agents

Silica materials are susceptible to chemical reactions when exposed to water in any form (i.e. gaseous or liquid). Figure 3.1 contains schematics of conditions that exist when silica is exposed to water, as well as water reactions with metal oxides. For silica, the exposed oxygen atoms acquire hydrogen atoms from either a hydronium ion (H_3O^+), commonly referred to as merely H^+ , or from dissolution products from water. The resultant is hydroxyl groups (OH^-) attached to the silica, and is known as network terminating silanol groups (SiOH). The figure also shows several configurations for siloxane linkages, a term used for an $\text{Si} - \text{O} - \text{Si}$ bonding link.

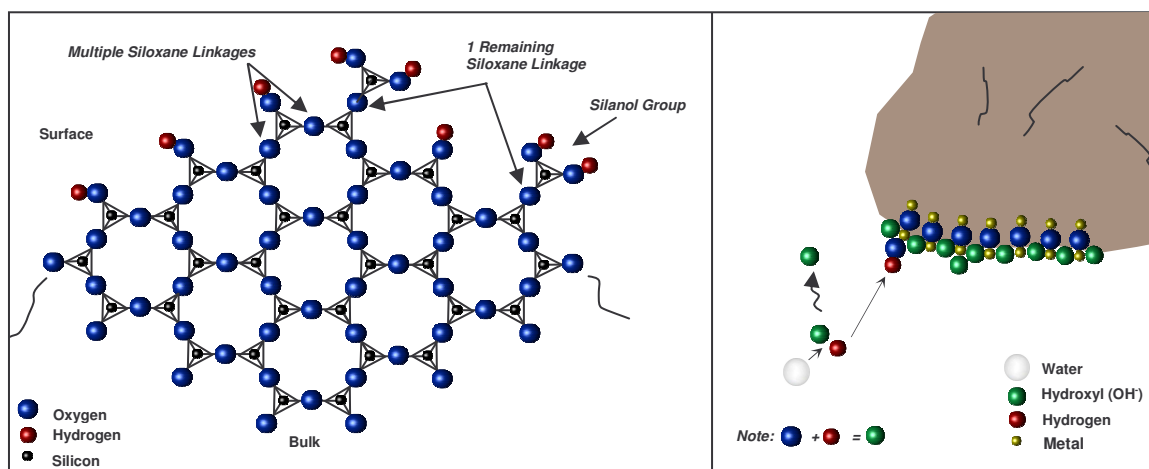


Figure 3.1: SiO_2 and metal oxide surfaces exposed to H_2O

The metal oxide behaves similar to silica materials by forming hydroxyl groups on the surface (MOH), where M can be different metal cations like tetravalent cerium (Ce^{4+}) and trivalent aluminum (Al^{3+}).

The term pH is often thought of in terms of ‘potential of hydrogen,’ meaning that the more hydrogen ions (H^+) that a solution contains, the more acidic it becomes, corresponding to values less than 7. A solution becomes basic when it contains excess

hydroxyl ions (OH^-), corresponding to values greater than 7. A solution pH of 7 corresponds to a neutral solution, or one that contains a relatively equal amount of hydrogen and hydroxyl ions [39].

The silica is subject to pH dependent protonization / de-protonization reactions according to the equilibrium equation below:



The equation begins to right shift, according to Cook, occurring at a pH of 2.2. Above this level, the surface exists as neutral and negatively charged. The right term in Equation 3.1 is a Bronsted base, meaning that it exists as a proton acceptor. Cook provides an equation (Equation 3.2 in Figure 3.2) for the percentage of bases (n_b) that exist for fully hydrated vitreous silica, shown as a terminating exponential curve in Figure 3.2. From this it is seen that pH of the solution will strongly affects the number bases available. This fact will be important in Steps 1 and 2 of the chemical tooth model.

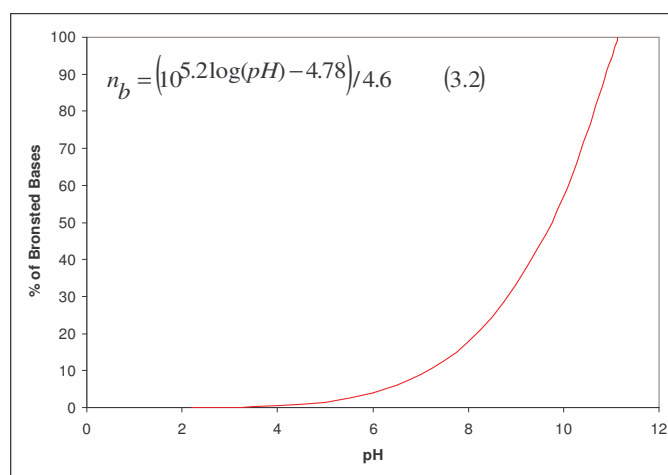


Figure 3.2: Percent of silica surface Bronsted bases

3.1.2 Steps in the Chemical Tooth Model

Steps One and Two

Step 1 of the chemical tooth model (Figure 3.3(a)) shows the formation of the condition described by Equation 3.1. A hydroxyl in solution obtains a proton (hydrogen) from the silanol group (SiOH) on the silica surface, forming the Si-O⁻ base and a water molecule. Step 2 (Figure 3.3(b)) occurs when the abrasive particle comes in contact with the glass surface. The oxygen of Si-O⁻ displaces a hydroxyl on the particle surface, freeing it to solution and forming an M - O - Si polar covalent bond. The process is termed condensation reactions and is of the form [37]:

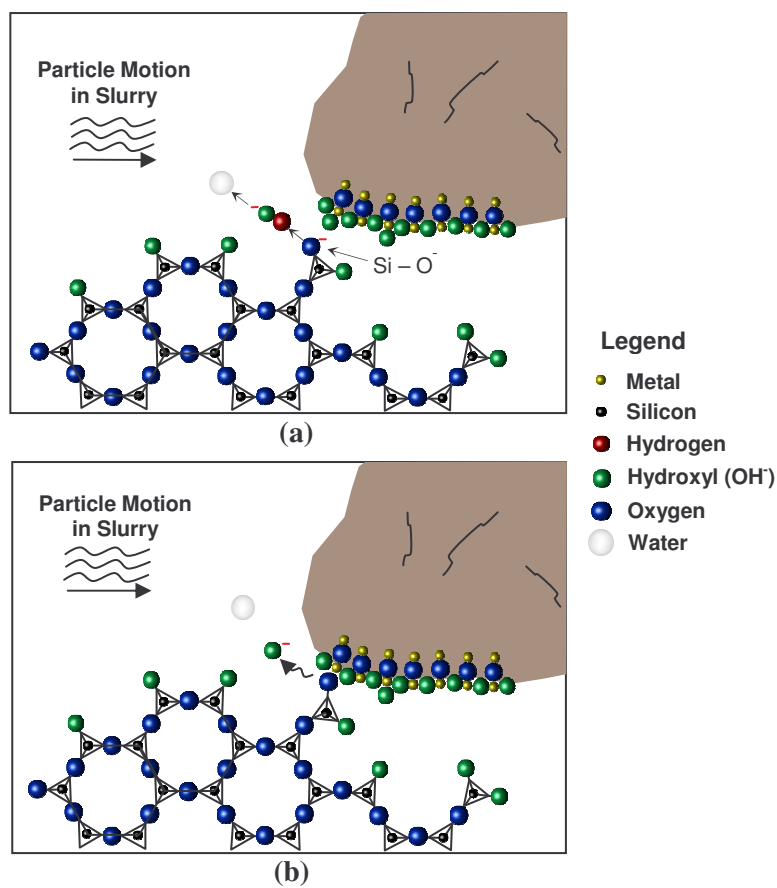
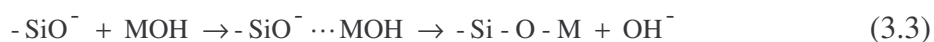


Figure 3.3: The chemical tooth model: (a) step 1 and (b) step 2

Step 3

Step 3, as outlined by Cook [35], has several possible outcomes. The abrasive particle is mechanically pulled across the glass surface, due to interaction between the moving workpiece and lap. If the M-O bond is weaker than the Si-O bond (Fig. 3.4(a)), then the silica tetrahedron is retained on the glass surface. If the M-O bond is stronger than the Si-O bond (Fig. 3.4(b)), then the silica tetrahedron will be removed from the glass surface and transported away on the abrasive particle.

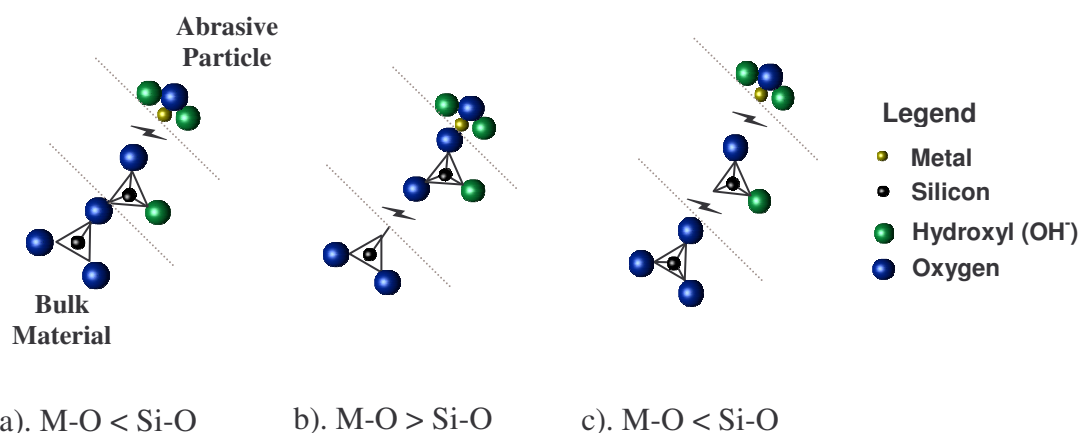


Figure 3.4: Possible fracture mechanisms for the chemical tooth model (Step 3)

Another possible removal mechanism is represented in Figure 3.4(c). If the M-O bond is weaker than the Si-O bond, and there is only one remaining siloxane linkage (Si – O – Si), the released energy from the M-O break can cause the last oxygen in the tetrahedron to rupture, producing an intermediate species.

Steps 4 and 5

Figure 3.5 shows what happens after the type of removal shown in Figure 3.4(c). Step 4 occurs when MOH is reformed on the particle surface by acquisition of a hydroxyl from solution and Si-O^- remains or reforms SiOH on the glass surface. The intermediate species obtains dissolution products from a water molecule and forms a free silicic acid molecule in the solution.

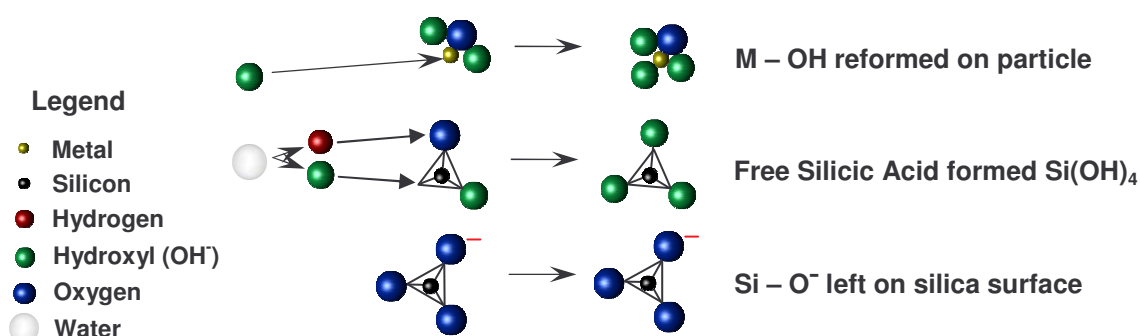


Figure 3.5: Steps 4 and 5 from the Chemical Tooth Model

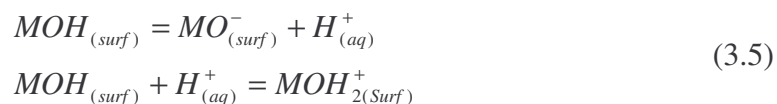
Step 5 involves the silicic acid floating away in solution, bonding to the particle surface, or bonding to the glass surface according to the reversal of a depolymerization reaction [35, 37]:



3.2 pH Effect on Colloidal Systems

One of the main influencing parameters to a colloidal system is the pH. As seen from Equation 3.1, the pH affects the surface charge on the silica surface. A similar effect is seen with the metal oxide abrasives. The particles can obtain a net surface charge through the ionization of the particle surface, which is pH dependent [40]. The surface charge density, or potential, is therefore controlled by the relative amount

potential determining ions, which is directly controlled by the pH in the case of metal oxides. Equation 3.5 shows the metal oxide protonization / de-protonization reactions [37, 41].



In words, acidic solutions with excess H^+ ions cause the particle to become more positive by protonizing the surface ($MOH + H^+ \rightarrow MOH_2^+$). Basic solutions with excess OH^- cause the particle to become more negative by de-protonizing the surface to form water ($MOH \rightarrow MO^- + H^+$). In this light, a pH level must exist where the net charge on the particle surface is zero, which is termed the point of zero charge (pzc). Figure 3.6 shows a theoretical surface charge curve of a metal oxide with a pzc of pH 7 [37, 40].

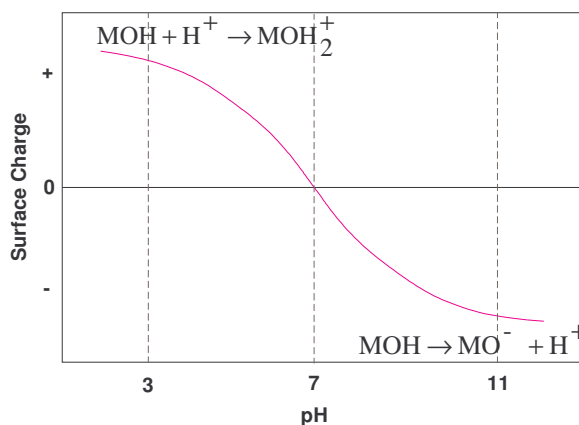


Figure 3.6: Theoretical surface charge dependence on pH for a metal oxide (after [37])

3.2.1 Influence of pH on Polishing Rates

Osseo-Asare (after Cook) provided experimental data on the polishing rate of silicate glass vs. pzc of several metal oxides used in polishing, conducted at a near neutral polishing slurry (see Figure 3.7). Note that under these conditions, ceria was the most

effective, which has a pzc of pH 6.8 [35]. This observation shows that maximum polishing rates occur when the substrate has a negatively charged surface and the polishing particles have a near neutral surface.

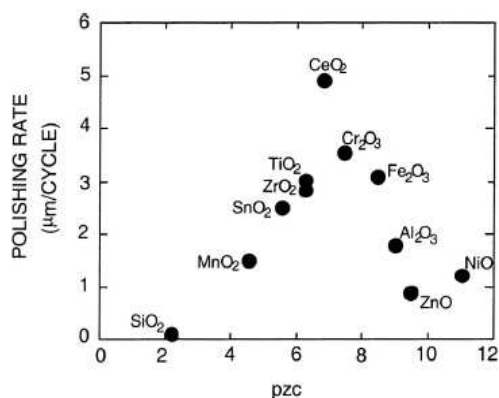


Figure 3.7: MRR vs. pzc for various abrasive particles ([37], Fig. 1, p. G652, after [35])

This phenomenon can be explained by examining particles with differing pzc.

Three curves are shown in Figure 3.8 with a constant solution pH of 7.

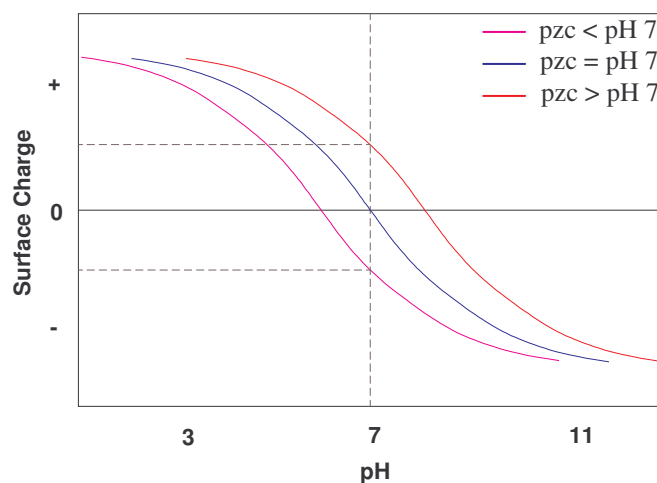


Figure 3.8: Theoretical surface charge curves for various abrasive particles with differing pzc (system pH = 7)

If the abrasive has a pzc lower than pH 7 (left curve), then the particle surface will be preferentially de-protonized at solution pH 7, leaving a negative surface charge (excess

MO⁻). A particle with pzc higher than pH 7 (right curve), then the particle surface is preferentially protonized at solution pH 7, leaving a positive surface charge (excess MOH₂⁺). Both cases have reduced neutral surface sites (MOH) which are required for material removal according to chemical tooth [35, 37]. Thus, the polishing slurry in the system can be adjusted to best match the pzc of the abrasive particle to aid in controlling the process.

3.2.2 Surface Charge and Zeta Potential

Measurement of the surface charge on abrasive particles is not a trivial task, but the zeta potential is a more readily measured parameter, which can give insight into the respective abrasive surface charge. When a particle exists in solution with a certain surface charge, oppositely charged ions (cations) within the solution migrate to the surface, creating a dense layer around the particle surface, termed the Stern layer. Then additional charged particles migrate around the Stern layer and form a diffuse cloud around the particle. The whole assembly has been termed the electrical double layer (EDL). Inside the EDL, there exists a plane of shear, where when the particle is moved, the ions inside the shear plane stay with the particle, and the ions in the diffuse layer are retained by the bulk fluid. The electric potential at the shear plane is termed zeta potential [40]. A schematic of the phenomena is shown in Figure 3.9.

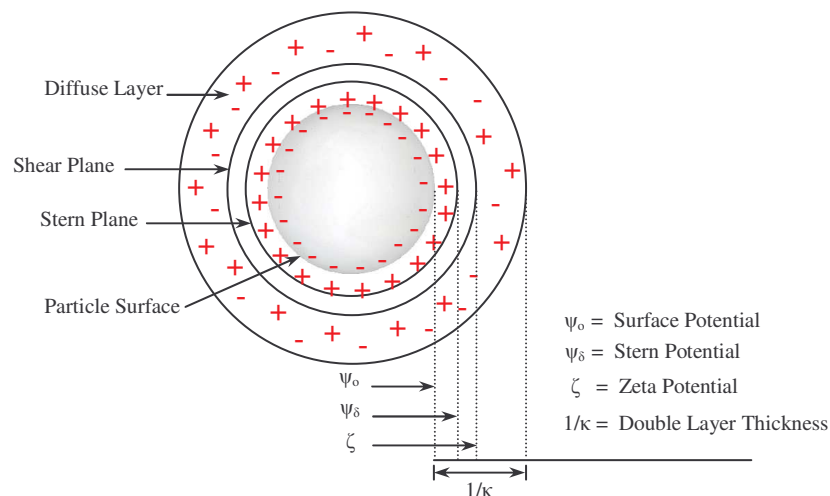


Figure 3.9: Solution particle acquired charges (after [42])

One important point to make is the delineation between terms often used in the description of colloidal systems, the point of zero charge (pzc) and the isoelectric point (iep). These terms could be mistakenly interchanged, but they are different. The pzc refers to the pH of the solution where the particle surface has no net charge. The iep refers to the pH where the zeta potential is zero. The most common method of zeta potential measurement is examining the electrophoretic mobility, which is measurement of the migration rate of particles that are subjected to an electric field [43]. Regardless of the charge value that slurry abrasive manufacturers use, the important point to retain is that adjustment of solution pH will directly affect the relative charge exhibited by the particle.

3.2.3 An Aside On Abrasive Slurry Dispersions

With an understanding of particle charge density, and specifically zeta potential, the charges associated with the dispersions described in section 2.1.2 can now be expounded upon. Colloidal systems can become unstable when the pH of the solution approaches the pzc of the suspended particles. Under these conditions there exists a

potential for the particles to agglomerate into larger clumps, known as flocculation, which occurs when the surface potentials are low enough for the moving particles to overcome the repulsive forces and bond together. A general rule of thumb for solution stability is a zeta potential of ± 30 mV. Methods to prevent flocculation include charge stabilization by adding potential determining ions or charged polymeric chains to make the particles preferentially positive or negative. Another method is the addition of polymers to the solution, which attach to the particle surface and physically prevent agglomeration by steric repulsion [40].

In reference to the Nanophase products used in this work, three of the ceria slurries (CE-6080, CE-6082, GP-18HD) can be considered charge stabilized, in that they contain negatively charged polymers that act to electrostatically repel individual particles. As developed, these particles are considered anionic (e.g. left curve in Figure 3.8) in recommended polishing pH values of 7-12 [10]. Thus, flocculation is prevented by keeping a sufficiently large negative zeta potential. As a result, the pzc of the system should be below pH 7, although the actual value is not known. Future measurements by Nanophase of zeta potential will be supplied when it becomes available in early 2007.

The fourth polishing dispersion (CE-6086) can be considered non-ionic because of the zero charged polymeric coating applied to the particles, which prevents flocculation by steric repulsion in the range of recommended polishing conditions (pH 4-11) [11]. It is important to note that these polymer additives are thought not to directly interfere with the particles ability to polish, as they only serve to prevent flocculation in the colloidal system. However, the effects will nonetheless be investigated.

3.3 Important Research Dealing with the Chemistry of Polishing

After publication of the method of chemical-mechanical removal by Cook, research began to understand the implications. This research is continuing today and is the underlying basis for the current work. However, it is important to understand the work that others have done. An extensive literature review was accomplished for this thesis and some of the more important papers findings are summarized here.

Hoshino

The chemical effects on polishing, and a proposed twist to the Cook model, was offered by Hoshino, et al [44], who performed ceria polishing of SiO_2 films. Through IR spectroscopy, it was determined that polishing changed the surface structure of the thin films, but the surface returned to a similar pre-polished condition when cleaned with an $\text{HNO}_3/\text{H}_2\text{O}_2$ bath. The noticed IR peak shift was attributed to Ce-O-Si bonding on the surface because the acid bath would dissolve the cerium oxide, but would not break down the silica bonds. The liquid phase of the polishing waste (after centrifugation) was examined and the ratio of silica to ceria was similar to the measured concentration of cerium and silicon. If material had been removed primarily by silicic acid formation, as Cook postulated, then there should have been a much higher concentration of silicon versus cerium in the polishing byproducts. Thus, it was speculated that SiO_2 must have existed as a lump on the polishing particles instead of silicic acid in solution. The proposed model has the basic features of chemical tooth, only differing in speculation that silica accretion on the particle surface is the dominant removal mechanism, versus the formation of silicic acid being dominant.

There are some points to note about this model. It assumes that the silicic acid would stay in solution, but according to chemical tooth, it can also rebond to either the polishing particle or to the glass surface. Also, Cook stated that silicic acid formation and subsequent removal was likely the primary mechanism. However, he also describes a mode that will allow for direct abstraction of the silica tetrahedron from the glass surface. Hoshino describes a similar process, only he shows multiple tetrahedra removal through different bonding sites on the particle surface. Cook does not refute this; he only states that a single Si-O-M bond would not be capable of removing multiple tetrahedra. Although there are some disagreements, the paper still highlights the importance of the chemical aspect of polishing.

Abiade and Choi

Abiade and Choi [45] studied pH effects on the polishing of silica thin films deposited on a silicon substrate. In this work, zeta potential of the ceria based slurries were measured along with the respective polishing rates. It was found that maximum material removal occurred at pH ~ 6, which was also the measured iep of the ceria slurry. Low removal rates were generated in acidic conditions and intermediate removal rates were obtained at basic conditions. The higher removal rates at the elevated pH levels were attributed to the enhanced dissolution of the silica in the corrosive environment.

Suphantharida and Osseo-Asare

Suphantharida and Osseo-Asare [46] studied zeta potential effects and silica adsorption on ceria solutions. The experiments did not use polishing slurries, rather solutions of ceria particles with varying amount of silicate ions added to determine end

effects. However, the experiments are directly comparable to the conditions found in polishing. Several interesting observations were made in this paper. First, it was shown that the zeta potential curves shift left with increasing concentrations of silicate ions in the pH range of 2-12. This shift showed that the pzc of the ceria particles, with increased addition of silicate ions, approached that of silica. For this to occur there would have to be substantial accretion of silicate ions on the ceria surfaces.

Another important observation was that maximum adsorption was found to take place near pH 9. At this level, both the silicate ions and ceria particles would be negatively charged and would be expected to repel one another. Thus, it is rationalized that the two species must be chemically bonding, versus bonding through charge forces. This observation tends to suspect that maximum removal rates would occur at pH 9 versus the chemical tooth prediction of pH 6.8.

Cumbo

Cumbo, et al [47], studied pH effects on the polishing of fused silica, BK7 borosilicate glass, and SF6 dense flint glass. Particle size and zeta potential measurements were made of three different commercial slurries (CeO_2 , m- ZrO_2 , and n- Al_2O_3) used in a slurry recirculation polishing system. It was shown that, with the exception of the CeO_2/SF_6 combination, the maximum removal rate occurred at the conditions where the particle pzc was closest to the slurry pH (i.e. pH 7 for CeO_2 , pH 4 for ZrO_2 , and pH 10 for Al_2O_3). This seems to support the Cook model, but it was shown that removal rate predictions with the chemical tooth model did not always correlate with experimental results when the glasses were subject to solutions that were corrosive to the glasses (i.e. acidic to neutral for SF6 and neutral to basic for BK7).

Of greatest interest to the scope of this thesis is the fact that average ceria particle size increased for neutral and acidic solutions, and decreased for basic solutions during polishing. This could be an important factor in surface finish results, since the current work will utilize a slurry recirculation system. For all combinations of particle-glass interaction, it was found that fluid pH and particle pzc is the adjustable parameter which can influence the polishing process. Additionally, they noted the chemical component could be comparable, or even dominate, the mechanical forces [47].

Tesar

Tesar [48], et al, also studied the effects of pH on the resulting surface finish. The trends on MRR are also highlighted, via the calculated Preston Coefficient, which has mass loss as the only variable. The study found that silica polishing with Hastilite PO brand ceria slurry produced higher MRR and better surface finishes at a pH of 4 versus a pH of 7. When silica was polished with Opaline (a higher purity ceria slurry) at pH 4, the removal rate was much lower, but the surface finish was nearly exactly that achieved with Hastilite at pH 4. Regardless of the removal rates, the work showed that higher quality silica surface finishes could be achieved with low pH ceria slurry.

This observation disagrees with Cumbo's findings. However, the Cumbo paper offers an explanation that the probable difference is that Tesar dispensed the slurry at low rates (1.2 mL/min) in a non-recirculating system versus their flow rates of 3 mL/s in a recirculating system. This potentially negated the buildup of silica chemical species within the solution and prevented agglomeration of the particles [47]. Relevant findings of both papers are provided in Table 3.1.

Table 3.1: Comparison of experimental parameters, from [47] and [48]

| | Glass | CeO ₂ Slurry Brand | Protonizing Agent | De-Protonizing Agent | Polishing Pressure | Results |
|-----------|--------------|-------------------------------|-------------------|----------------------|-----------------------|---|
| Cumbo [X] | Fused Silica | Traselco | Hydrochloric Acid | Sodium Hydroxide | 40 gf/cm ² | -- Higher MRR at pH 7 -- Surface Finish approximately the same at pH 4-10 |
| Tesar [X] | Fused Silica | Hastilite / Opaline | Citric Acid | N/A | 26 gf/cm ² | -- Higher MRR at pH 4 (Hastilite), no comparison for Opaline -- Surface Finish best at pH 4 for Hatilite and Opaline |

It is seen from the last two examples that polishing experiments are difficult to directly compare, but they can offer some insight into expectations from a particular setup. Regardless of the inability of direct comparison, the importance of chemistry in the polishing process is shown. By directly controlling variables that influence the chemistry, more insight can be drawn into the removal mechanism.

3.4 Motivation for Current Work

Optical polishing of glass continues to be an essential process for many different applications. A good deal of experimentation has been conducted over the years to attempt to understand the process of glass polishing. If a comprehensive model existed, then steps could be taken to maximize parameter effectiveness and reduce the polishing production time (i.e. savings to cost/schedule/performance). However, a notable decline in the interest of glass polishing mechanisms was noted on review of the literature. A probable cause is the increased interest in CMP, which is a critical step in the manufacture of integrated circuit chips. This is a huge industry that brings with it large amounts of money, and subsequently, research interest.

This thesis will attempt to provide some interlinking data that can be used to justify existing models of material removal, namely the dominance of either a mechanical

or chemical material removal model. A new hypothesis will not be proposed, but some amount of justification will be provided. Previous experiments that look at the role of chemistry in glass polishing [27, 35, 36, 37, 44, 46, 47, 48] offer some amount of disagreement as to the optimum slurry conditions with regards to material removal and surface finish. Through variation of several easily controlled parameters (particle size, density and pH), attempts will be made to understand these optima, and help to delineate factors influencing the chemical and mechanical models.

The effects on surface finish will also be heavily addressed. With an increased need for low surface roughness optics, as in x-ray and enhanced ultra-violet applications, it is imperative to understand the impacts of changing system variables. The results will also be used as baselines for ongoing theoretical modeling being conducted by Dr. Ed Paul from Stockton College, NJ.

CHAPTER 4: EXPERIMENTAL PROCEDURES

A polishing process may be set up with minimal equipment, the main apparatus being the polishing machine. For this research, a production quality Strasbaugh nFocus precision polishing machine was used (Figure 4.1). The machine is capable of accurately controlling the spindle and eccentric arm speeds. The pressure to the workpiece is applied through a pneumatic cylinder ram. It was found that application of pressure via this mechanism was not optimal, and will be discussed in detail in section 4.3.

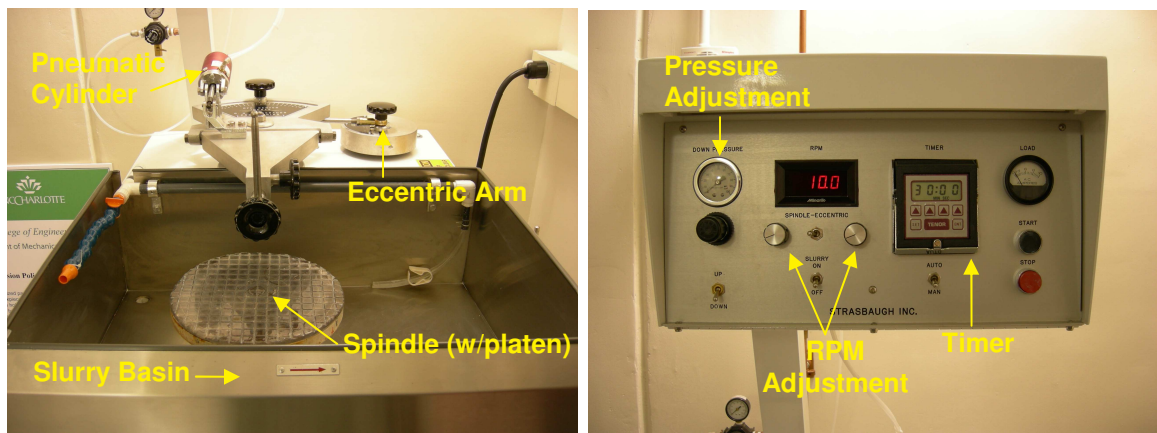


Figure 4.1: Major components of the Strasbaugh nFocus polishing apparatus

4.1 Material Preparation

It is important to describe the methods used to prepare the materials and measure the results of the various experiments. Many of the published papers on polishing do a reasonable job of describing most aspects, but invariably, some of the process parameters

needed to reproduce the experiments are omitted. In an effort to avoid this, complete details will be provided for the experimental process.

4.1.1 Pitch Tooling

As described in section 2.1.1, Acculap synthetic pitch was used for the majority of the experimentation. Two pitch tools were manufactured to match the abrasive slurries, one for the larger abrasive slurry (750 nm) and one for the small abrasive slurries (40 and 20 nm). Several iterations of tools were made to ensure uniformity. Manufacture of the pitch tooling consists of three basic steps: pouring, channeling, and run-in.

Pouring the Pitch Tool

To create a pitch tool, the viscosity of the pitch is lessened through heat addition and then poured onto a cast iron or aluminum platen. The heat can be introduced by immersion of a pitch container in a water bath, or through a convection oven. For the water bath technique, the pitch was broken up and placed in a glass container, which was immersed in another water filled container resting on a laboratory hot plate. Using this method required constant stirring of the pitch to heat thoroughly, due to the open air heat sink of the glass container, which led to the development of bubbles. As the tool cooled, the bubbles would create blow-outs on the tool surface. Several tools were made in this manner, each having the same basic surface. The voids are undesirable because it effectively reduces the amount of surface area available for polishing. It is important to note that the voids would likely have little effect on the resulting surface finish of a workpiece, but could influence removal rates. The convection oven technique was used because it reduced the amount of stirring necessary, since it was heated in all directions, and resulted in almost no bubble formation.

The platens were prepared by thoroughly cleaning the surface with acetone and constructing a dam wall out of duct tape to provide the desired tool thickness of 0.5 in (1.27 cm). The only purpose of the dam was to prevent the pitch from flowing off of the tool, since the viscosity at pouring temperature was comparable to thick syrup. Once poured, the tool was left on a flat surface and allowed to cool overnight.

Channeling the Pitch Tool

It is critical to have channels in any type of polishing lap to promote the flow of slurry to and transport material away from the workpiece. The shape of the channels, as mentioned previously, can have an effect on polishing conditions. Opticians will likely develop a feel for what patterns should be used based upon application, but the concept is still very subjective. For this work, a simple square grid pattern was employed, with a square channel cross section (see Figure 4.2).

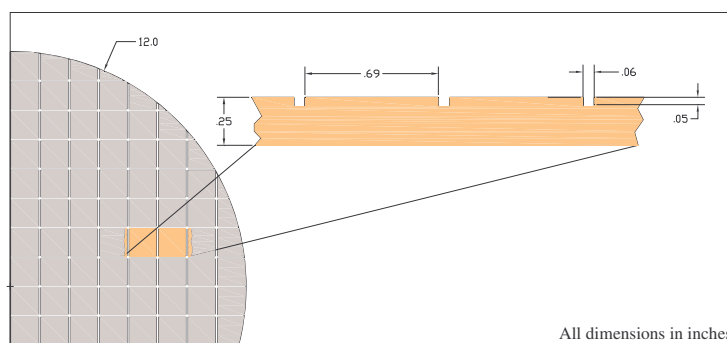


Figure 4.2: Pitch tool pattern with cross-sectional cutaway

The channels were formed by ‘cutting’ the pitch through successive passes of a coarse tooth saw blade typically found on horizontal band saws. Both fine and course teeth blades were tried, but it was found that the fine tooth blade tended to clog up with material rapidly, reducing the amount of material removed. This not only increased

production time, but increased the risk of the blade catching an adjacent facet, causing excessive chip out of the polisher. A typical tool took 3-4 hours to channel, with time increasing depending on the channel depth. Figure 4.3 shows a completed pitch tool.



Figure 4.3: Typical channeled pitch tool (12 inch diameter)

Run-In of the Pitch Tool

After the tool is built, it is necessary to break it in to a level suitable for polishing. A piece of glass is first heated under hot water and then pressed against the surface, moving in circular patterns. This step helps to remove any protruding chips and flattens down any high spots.

The next step is to build up a layer of abrasive particles on the tool surface, accomplished by simply polishing a representative piece of glass with the desired slurry. A pitch tool is considered ready for use when a visible crust develops on the polishing surface, which is indicative of abrasive particles embedding in the surface. The 750 nm tool developed a defined crust at 4 hours polishing time. The small abrasive tool (40 and 20 nm abrasive) also developed a crust, but it was much finer and difficult to see due to the relative size of the abrasives embedded in the tool. To ensure an effective run-in cycle, the tool was conditioned with a 40 nm abrasive slurry for 12 hours, 3 times that of

the 750 nm tool. During this period, the crust was not visibly changing and thus considered to be at a point to begin experimentation.

4.1.2 Abrasive Slurry

The slurries were prepared as close as possible to the Nanophase provided guidelines. Before diluting the solution, the container was shaken by hand until there was no visible sedimentation on the interior surface (~5-10 minutes). To facilitate good particle distribution, the container was mounted on a sufficiently violent vibration table for an additional 20 minutes [49]. The contents were then diluted with 18 M Ω filtered de-ionized (DI) water at the ratio of 10:1 water to slurry. The DI water was obtained from the UNCC clean room system located in the Cameron Applied Research Center.

Once diluted, other properties of the slurry could be varied dependent on the experiment, or used as mixed. When modified, the slurry was poured into a mixing container on a magnetic stirring table. The pH was measured by a calibrated Daigger 5500 pH meter, which provided the pH and temperature of the solution. The density was measured by an Anton-Paar DMA 35N density meter, which provided density and temperature. The resolution of the pH meter was .01, and 0.1 mg/cm³ for the density meter. Adjustment/verification of pH and density of the slurries was made before each experimental procedure. Figure 4.4 shows the slurry adjustment workspace.

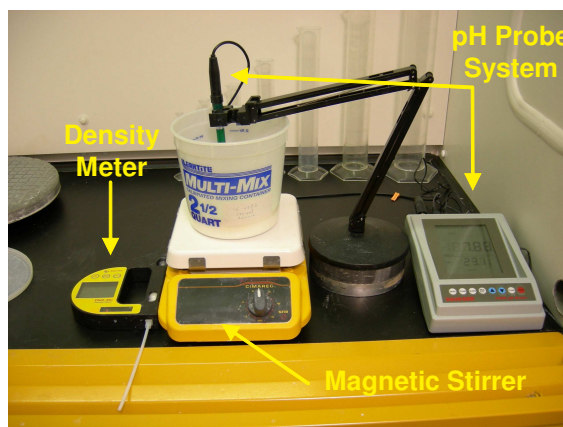


Figure 4.4: Density and pH adjustment area

The pH was controlled by adding nitric acid (HNO_3) to increase acidity and sodium hydroxide (NaOH) to increase basicity. These materials were used because they are non-reactive with both silica glass and cerium oxide, and recommended by the slurry manufacturer [49]. The materials were obtained from the UNC-Charlotte chemistry department, in concentrations of 6M nitric acid and 3M sodium hydroxide. The different molarities had no operational impact, except that a certain amount of acid would shift pH more than the same amount of the weaker solution base.

4.1.3 Workpiece Material

In order to adequately capture the polishing variable effects, the starting surfaces needed to be polished to a relatively high degree. The value chosen was around 1 nm R_a , as measured with the 2.5X Michelson objective on a white light interferometer. Polishing to this level was accomplished with Opaline and a polyurethane pad, and then a final polish with CE-6080 (750 nm) ceria slurry on pitch. The as received surfaces were very different, with the quartz having a decent ground surface and the fused silica having a surface more indicative of being sawn with a light grinding.

The density of each material was also checked by weighing the pieces with an Ohaus Adventurer (Model AR0640) analytical balance (resolution = 0.1 mg), and the diameter and thickness determined by measuring with a Brown and Sharpe (MicroVal 343) coordinate measuring machine (CMM). The results were in agreement with the manufacturers reported values. This step was needed to generate the inputs to the mass removal rate calculations (i.e. polishing area and mass). This calculated value could then be used to compare with the step height method of removal rate measurement used in this work, and which is described in the following section.

4.2 Material Removal Rate Quantification Method

Measurement of material removal rates provide critical insight into how fast the process is proceeding and is important when a certain amount of material has to be removed (e.g. in chemical-mechanical planarization of silicon wafers). Typical methods of measurement are centric to the mass, by weighing the sample before and after polishing. While this method is viable, it is subject to some potential errors such as cleanliness of the part after exposure to the slurry and water absorption by the workpiece. The mass of silica materials can even fluctuate as a function of humidity. To address that concern, a different measurement technique was used to determine material removal rates based on the height difference between a lapped recess and the polished surface.

4.2.1 Step Height Material Removal Rate Method Considerations

The basis of this concept is simple. The recess method allows for material removal from the glass surface, while the bottom of the recess is left unaffected. Several key considerations need to be made however. The recess depth should be much larger

than the diameter of the particle to prevent the risk of particle loading on the recess bottom. If the MRR is high, then the recess also needs to be sufficiently deep enough to prevent it from being polished out. The lap type should also be a consideration. If a pad lap with asperities is used, then there is a risk of particles on the end of these asperities interacting with the recess surface on a recess with insufficient depth (see Figure 4.5).

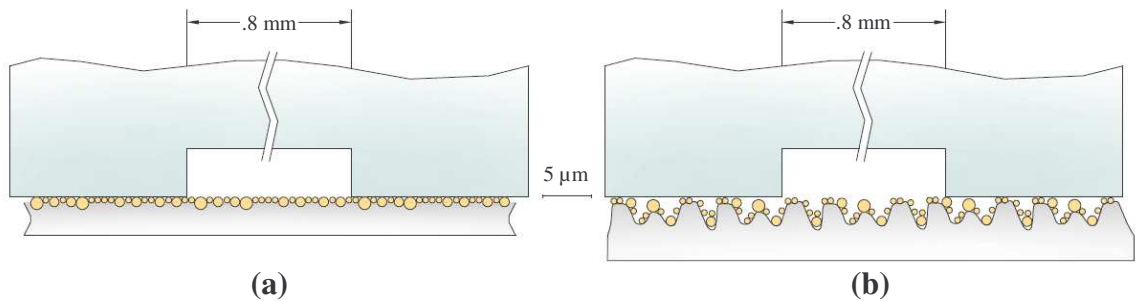


Figure 4.5: Polisher interaction with recess: (a) pitch and (b) polishing pad

To verify that the recess surface was not affected by the polishing process, several photomicrographs were taken at various polishing steps. Figure 4.6 shows the pictures taken, with the initial depth being 13.6 μm. Upon close inspection of the tooling marks, it was seen that the recess surface was unaffected by the polishing process.

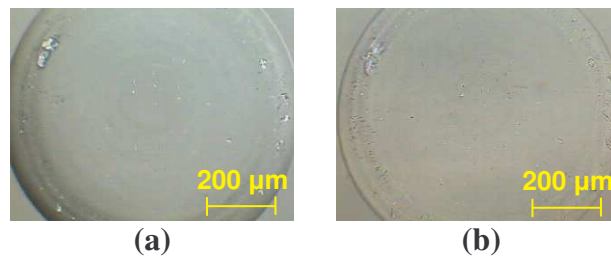


Figure 4.6: Photomicrographs of Recess Surface: (a) Initial and (b) after 2.554 μm removed

The procedure used for this thesis achieved recesses on the order of 5-15 μm in depth (dependent upon hardness of the workpiece), while retaining a good surface finish

on the recess bottom. Depending on removal rates, a 10 μm of depth can last for many hours of polishing. Depth of the recess is also important due to the interferometric measurement system with step height application. The scan length of the interferometer was 100 μm maximum in the z-direction, which necessitated that the recess be less than that value. However, it was found that recesses above 20 μm caused problems, potentially due to light adsorption resulting from the higher aspect ratios. The recess dimensions were also a concern since the max field of view on the interferometer with a 2.5X Michelson objective was 2.82 x 2.11 mm. The recess needed to be sufficiently large to measure the bottom surface, but small enough to allow a large enough of a reference on the polished surface. The bottom surface of the recess also needed to be flat and specular in order to make measurements with the interferometer.

4.2.2 Step Height Creation

Several different methods to create a recess were attempted with varying results. Most of the methods attempted resulted in recesses with fairly rough bottom surfaces, which caused large amounts of light scattering when viewed with an optical microscope, and thus were generally too diffuse to measure with the interferometer. Some of the methods attempted were diamond drills, diamond wafering blades and surface grinding wheels, and oxygen free copper lapping rods with Opaline, a high purity brand of ceria, or diamond paste.

The most effective method of recess creation found was to use a hardened steel rod, which had a 1/32" diameter (.794 mm). The tool was conditioned by continuously lapping a piece of scrap glass with an Opaline slurry mix (1 μm average particle size, mixed 50 g/500 ml) for several hours. Hardened steel seems, at first, to be an odd choice

for a lapping material. Typical lap materials are usually much softer than the workpiece (e.g. copper) to allow the abrasive particles to embed in the lap. As described above, the copper rod left a diffuse recess surface. The hardened steel lap tool restricted the lapping process, causing it proceed much slower. The result was that the abrasives didn't imbed in the lap tool, but instead rolled between the spinning tool and the glass surface. This micro-grinding action produced a surface that was both flat and specular. Figure 4.7 shows a comparison between lapping with steel versus copper.

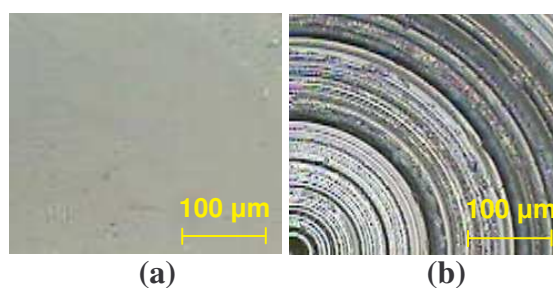


Figure 4.7: Recess surface lapped with (a) steel/opaline and (b) copper/diamond

Various slurries were needed to effectively lap a recess in the different glasses. Opaline worked well with Fused Silica, with a lap rate of approximately $0.5 \mu\text{m}/\text{min}$. For quartz, $0\text{-}0.2 \mu\text{m}$ diamond paste worked well but proceeded at a much slower rate, approximately $0.08 \mu\text{m}/\text{min}$.

The recess was created on a standard milling machine running at 1000 rpm. The lap tool was held in place with a zero force chuck (see Figure 4.8), which allowed for variable and controlled pressure in the z-direction. This was an essential tool, since a standard chuck would give much less feedback on how much induced loading was being applied to the glass surface. Only slight hand pressure was used to create a recess.



Figure 4.8: Lapping tool mounted in zero-force chuck

4.2.3 Step Height Measurement

The step height measurement was taken with a sub application in the MetroPro™ software controlling the interferometer. Masks were created to segregate the test surface (recess) and the reference surface (remaining portion of the FOV not occupied by the recess). The recess could be aligned to the test masks in varying ways. The primary method used in this research was by taking advantage of the visible fringes at the bottom of the recess. Due to the fact that the recess was created using a rapidly spinning rod, there is a definite morphology associated with the bottom of the recess. This translates into a defined fringe pattern when focused on the interferometer. Since there is no loading applied to the area during polishing, the fringes provide a definite method of aligning the mask. Another method would be to simply center the test mask in the recess visually by utilizing the video monitor. Figure 4.9 shows the mask aligned with the recess. The mask areas are in purple and the silica material is in shades of gray.

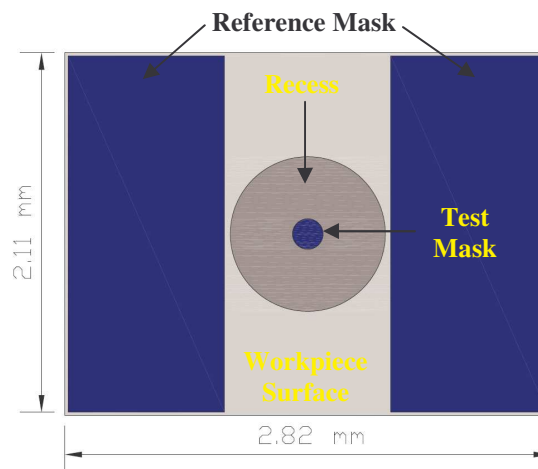


Figure 4.9: Mask alignment to recess for step height measurement

Once the mask is aligned, care was taken to ensure that the measurements were taken under similar conditions. The software outputs values of the tip/tilt (roll/pitch) of the measurement table and allowed consistency between measurements. A fiducial mark was also placed on the side of the glass to achieve proper alignment when loading. Figure 4.10 shows two sequential measurement outputs. Note that the areas not contained within the masks are not shown in the output.

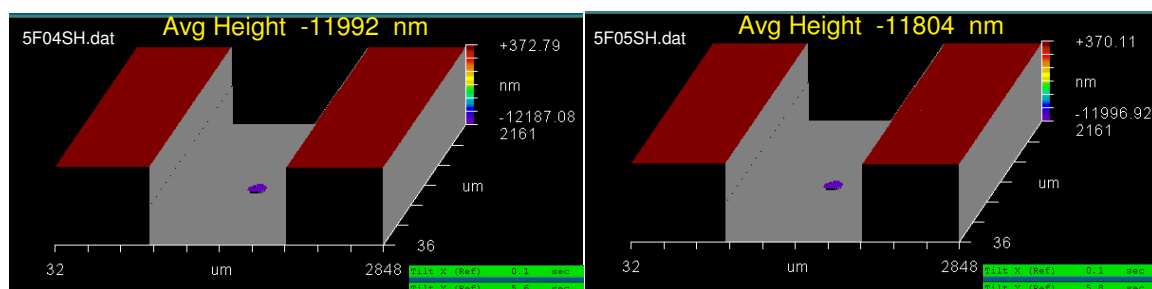


Figure 4.10: Sequential Polishing Experiment Output ($\Delta = 188$ nm)

4.2.4 MRR Measurement Method Verification

To prove the viability of this method to measure removal rates, it was necessary to compare results with the more common method of mass removal. Fused silica was polished on pitch with CE-6082 (40 nm) slurry kept at a constant pH of 7. The polishing pressure and relative velocity were kept constant at 39.8 gf/cm² (equivalent to applying a 4 lb dead weight load) and 9.4 cm/s, respectively. These polishing runs were coupled with another experiment examining the effect of slurry density on removal rates, so the density was varied from 1.005 – 1.035 g/cm³. Discussion of the slurry density effects are in Section 5.3. Two 1-hour runs were performed at each of four densities for a total of 8 experiments.

The mass of the glass was measured before and after polishing with an Ohaus Adventurer analytical balance (Model AR0640) with a 65 g capacity and a resolution of 0.1 mg and the step height measured with the method described previously. The workpiece was thoroughly cleaned and the surfaces were wiped with acetone before weighing. The removal rate was obtained using Equation 4.1, shown below, where ΔM is the change in mass, ρ is the glass density, A is the polishing surface area, and Δt is the polishing time.

$$MRR = \frac{\Delta M}{\rho A \Delta t} \quad (4.1)$$

Figure 4.11 shows a comparison of the two methods. Both exhibit the same trends, however there are some differences. At three of the four density levels, mass measurement is lower than the step height method. This could be due to water adsorption by the piece. If water is retained, the actual mass will be reported high and would effectively decrease the removal rate. The experiment at 1.015 g/cm³ shows the two

methods are in basic agreement. Based on these facts, it was determined that the step height method would give a better prediction of the MRR, with less influencing factors.

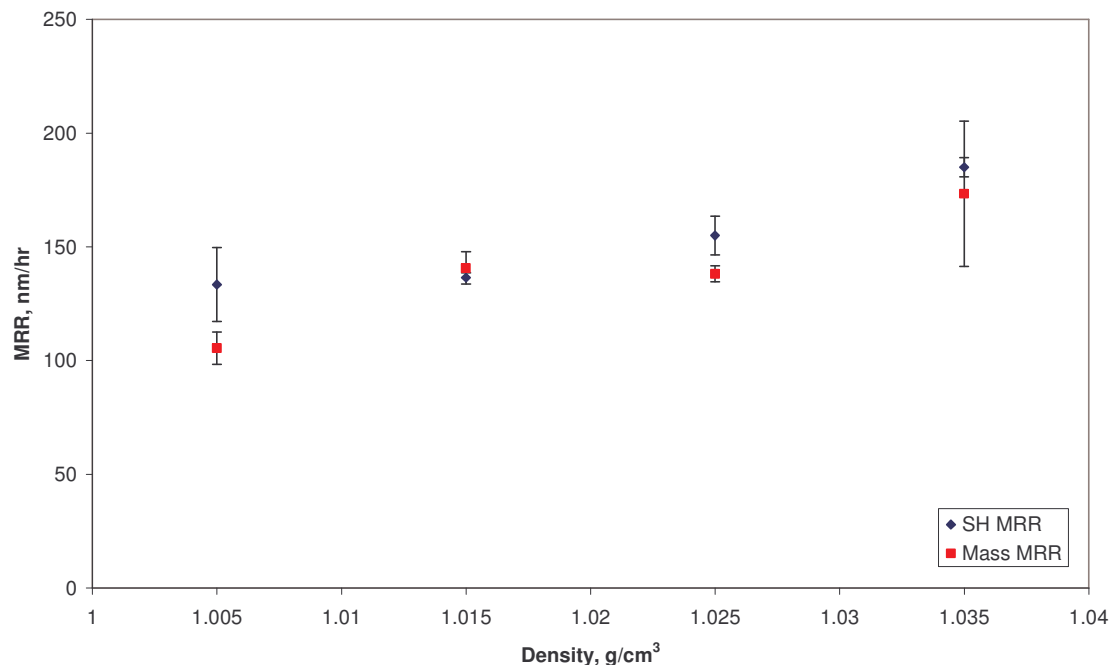


Figure 4.11: Step height and mass removal rate method comparison

4.3 Loading Conditions During Polishing

A review of the Preston and Brown/Cook equations (Equations 2.1 and 2.2) show the direct dependence of removal rate on polishing pressure and speed. This fact has been demonstrated by the majority of polishing papers, in some form or another. Because neither of these was a chosen variable for the experimentation in this work, a review of their impacts was necessary. Polishing trials examining these two variables were conducted as both a qualitative experiment and a learning experience, to aid in becoming familiar with the intricacies of the polishing process.

4.3.1 Pressure and Relative Velocity Experiments

Two fundamentally different substrates were chosen for these experiments, crystalline quartz and Zerodur[®], which is a glass ceramic material containing both crystalline and amorphous phases. Dissimilar materials were chosen because the polishing rates would be substantially different. The mechanical properties of the two materials are highlighted in Table 4.1.

Table 4.1: Mechanical properties of quartz and Zerodur[®]

| | Quartz | Zerodur [®] | Units |
|--|-------------------------------------|----------------------|------------------------|
| Density ^{a,b} | 2.65 | 2.53 | g/cm ³ |
| Young's Modulus ^{a,b} | 103 [∥] (78 [⊥]) | 90.3 | Gpa |
| Poisson's Ratio ^{c,b} | 0.056 a | 0.243 | |
| Coef. of Thermal Expansion ^{d,e} | 9.91 | 0 ± 0.1 | x10 ⁻⁶ / °C |

a - Ref [21], b - Ref [24]

c - Calculated from theoretical equation provided by [23] using [21] data

d - Average calculated from [saywer] data in the range 0 - 573 °C

e - Highest typical value in operating range 0 - 50 °C

∥ - Parallel to the z-axis ⊥ - Perpendicular to the z-axis

The polishing lap was a polyurethane pad affixed to a cast iron platen. Opaline (cerium oxide) abrasive slurry (1 μm average diameter) was used and applied at a constant rate of 16 mL/min through a peristaltic pump. The polishing load was applied via the overarm pneumatic air cylinder on the polishing machine. Recess step heights were created in both surfaces and the preliminary step height data captured. The variable parameters were pressure applied to the workpiece and spindle/eccentric rpm. Each material was polished for one hour under appropriate conditions and the results are shown in Table 4.2. The 'baseline' loading condition represents a certain applied load,

and the percentage increase is simply an increase in the air pressure to achieve a higher load. This parameter has been made relative, and is only important in the fact that load seen by the workpiece has been increased.

Table 4.2: Results from variable load and lap velocity experiments

| | Loading Condition | Spindle Speed (RPM) | Ecc. Arm Speed (RPM) | Relative Velocity (cm/s) | Removal Rate (nm/hr) | Cp ($\times 10^{-14}$ cm ² /dyn) |
|----------------------|-------------------|---------------------|----------------------|--------------------------|----------------------|--|
| Quartz | Baseline | 10 | 10 | 8.25 | 408 | 2.800 |
| | 50% Inc | 10 | 10 | 8.25 | 418 | 1.912 |
| | 100% Inc | 10 | 10 | 8.25 | 690 | 2.369 |
| | 100% Inc | 10 | 20 | 13.5 | 727 | 1.525 |
| | 100% Inc | 20 | 10 | 18 | 978 | 1.539 |
| | 100% Inc | 20 | 20 | 19.5 | 1302 | 1.891 |
| Zerodur [®] | Baseline | 10 | 10 | 8.25 | 377 | 7.327 |
| | 50% Inc | 10 | 10 | 8.25 | 450 | 5.828 |
| | 100% Inc | 10 | 10 | 8.25 | 647 | 6.288 |
| | 100% Inc | 10 | 20 | 13.5 | 899 | 5.339 |
| | 100% Inc | 20 | 10 | 18 | 933 | 4.156 |
| | 100% Inc | 20 | 20 | 19.5 | 2684 | 11.035 |

The first three inputs for quartz and Zerodur[®] show that as load is increased, the subsequent material removal also increases. The last three inputs in each section show that as the relative velocity is increased, again MRR increases. The results make sense no matter which material removal mechanism is believed to be in action. In abrasive removal theory, higher loads mean larger penetrations and higher velocities mean more rapid material removal. From a chemical aspect, the higher loads may represent more reaction sites of the abrasive particle coming into contact with the workpiece and higher velocities translates directly into a faster plucking rate.

Preston's Coefficient (C_p) is also supplied. This value, albeit empirically derived, is sometimes used as a measure of the polishing efficiency of a given system. For this

work, C_p is calculated according to Equation 4.2 below, with MRR as the material removal rate, P the polishing pressure, and V_R the relative workpiece/lap velocity.

$$C_p = \frac{MRR}{P \cdot V_R} \quad (4.2)$$

4.3.2 Control Measures

With the knowledge that pressure and relative velocity can have large impacts on removal rates, control methods needed to be implemented to remove them as variables in the main experimentation set. Relative velocity was simple to control because of the digital readout and potentiometer control of the speeds of the spindle and eccentric arm. The load control proved to be more difficult. Loading conditions were measured in both static and dynamic conditions.

Static Loading

To better understand the load seen at the workpiece surface, a representative 3” diameter (7.62 cm) glass sample was mounted on a workpiece holder and in the polisher. With the swing arm positioned in the center of arc travel, an Ohaus bench scale (Model ES6R) was placed in between the glass workpiece and a 22” platen. Loading curves were generated from 5 to 40 psi pneumatic pressure at different positions on the quill extension and the scale values were recorded (See Figure 4.12). The results show that the applied loads are fairly consistent at the different extension points. However, these tests were static and there was still some concern as to the actual loads seen by the workpiece when polishing. Also, a condition was identified when tightening down the quill rod. Depending on the amount of tightening, the transmitted force to the workpiece varied by

as much as 0.5 lb_f. This was concerning in itself because a variable was introduced even before the pneumatic pressure was applied.

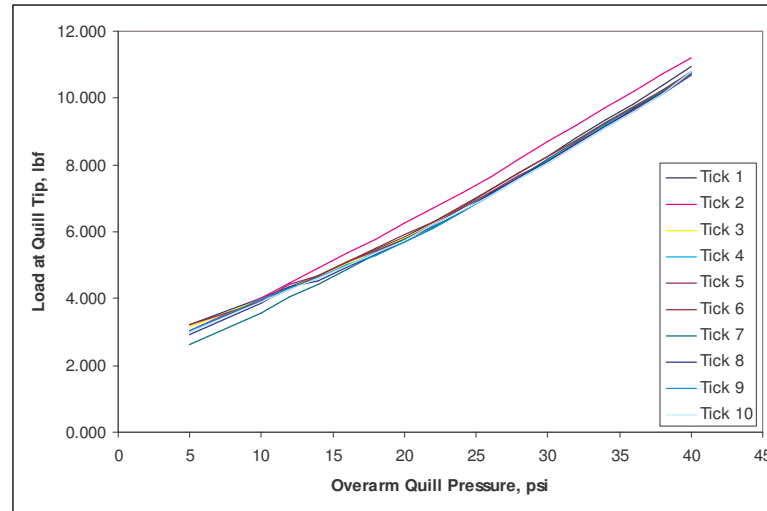


Figure 4.12: Polishing apparatus loading curve

Dynamic Loading

To answer the question of dynamic loading, a load sensing device was fabricated to generate loading curves associated with typical polishing runs (see Figure 4.13). This apparatus was designed to allow for either overarm quill or dead weight loading.

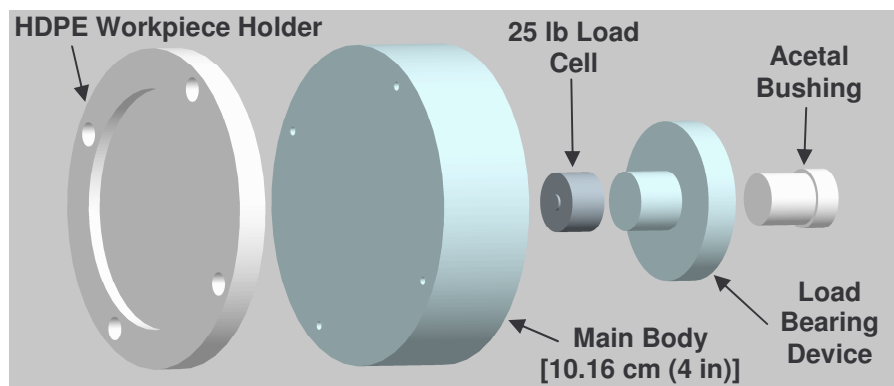


Figure 4.13: Schematic of the load sensing device

The device consists of a main body holder made of aluminum with a high density polyethylene (HDPE) workpiece holder. The HDPE holder serves as a quick method of mounting a workpiece without the use of optical wax or adhesives. The material is readily machinable, and a holder for virtually any dimension workpiece can be manufactured in about an hour. A 25 lb_f load cell (Omega Model LC302-25) was fitted inside a pocket along the centerline of the main body with a conduit channel for the wiring.

A load bearing device was manufactured and placed inline with the load cell, providing a platform to allow either dead weight loading or accept the overarm quill. An acetal bushing was manufactured to slip inside the load bearing device to provide a low friction environment for the quill rod interface. This design also provided the gimble mechanism needed in polishing to overcome variations in the polisher. If dead weight loading was used, the quill rod was placed inside the bushing but was not allowed to touch the bottom. This allowed the machine to move the workpiece across the polisher without inducing a load. If overarm pressure was desired, the quill rod was simply placed in contact with the bottom of the bushing.

A representative polishing test was performed on both pitch and a polyurethane pad. The pitch had approximately 7 hours of polishing time and can be considered completely conformed. A fresh pad was used and mounted on the flattest available platen. The platen flatness was measured on a CMM with a grid spaced measurement strategy totaling 160 measurement points. The resulting flatness value for the plane fit data was 19 μm.

CE-6080 (750 nm) slurry was used, mixed 10:1 and applied by an applicator bottle. The relative velocity was 8.25 cm/s, dead weight load was 4 lb (1.81 kg), and overarm pressure was adjusted from 5 to 20 psi (34.5 – 137.9 kPa). The workpiece was allowed to polish for 10 minutes before any data was captured. The load cell data was acquired using a National Instruments dedicated data acquisition card and processed with a Labview program. An example set of generated curves are shown in Figure 4.14.

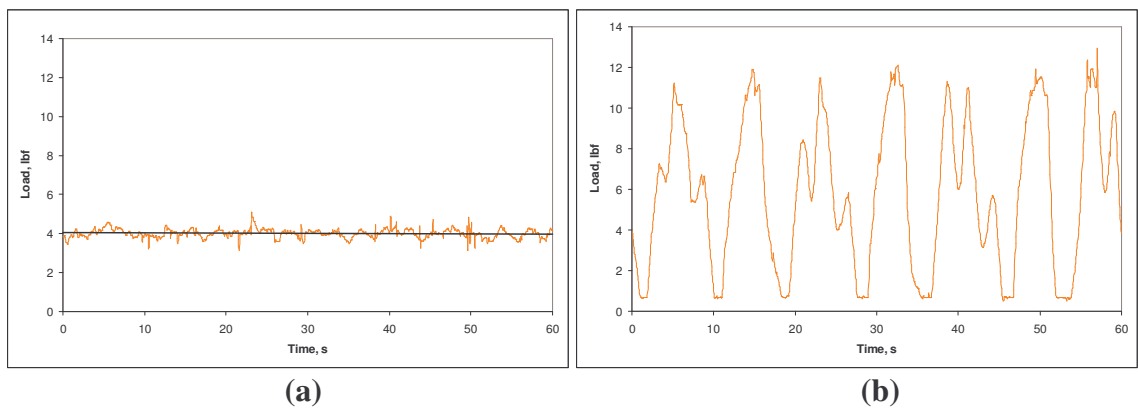


Figure 4.14: Loading curves with (a) dead load on pad and (b) 10 psi overarm pressure on pad

As the data show, using dead weight loading provides a more consistent load application during a polishing cycle. When the loading is applied via the overarm quill rod, there are significant loading fluctuations, varying by over 10 lb_f. The curves generated for pitch exhibited the same behavior. It is suspected that the pressure gradients seen are caused by misalignment of the overarm and the machine spindle. By adjusting the spindle motor mount, the misalignment could be reduced, but using the dead weights was just as effective and much simpler. The realization of the pressure gradient existence is important because typical dead load weighting is usually performed by adding weight directly to the overarm. This scheme is undesirable because the

misalignment would still be evident at the toolpoint. Thus, by using dead weight loading directly on top of the workpiece and preventing the quill rod from contacting the workpiece holder in the z-direction, another variable could be eliminated.

4.3.3 Constant Load Device

Because the HDPE holders were material specific, due to variable thickness, an adjustable constant load device was needed. To maximize space, a high density material was chosen, namely lead ($\rho = 11.34 \text{ g/cm}^3$) [50]. A large fishing weight was selected because the dimensions would allow placement and the weight matched the selected requirement for constant 4 lb (1.81 kg) load. Fishing weights are made out of a lead alloy, so the density did not exactly match that of lead, but was sufficiently heavy for its intended purpose. Five 0.5" (1.27 cm) diameter holes were drilled along the centerline of the weight. The center hole allowed the quill rod to pass through, and the remaining ones were used to calibrate the device for each piece of glass. Because the quartz HDPE holder weighed the most, the baseline calibration was set with this configuration. The main body, quartz HDPE plate, screws, lead weight and eight polyurethane caps (to hold in ballast) were placed on an Ohaus Ranger model bench scale. Number 6 lead shot was added to the outermost cavities until reaching the desired weight. The fused silica HDPE plate was then substituted and shot added to the interior cavities until the weight was again reached. With this configuration, the interior holes would be emptied when polishing with quartz, and the shot added back when polishing with fused silica. The constant load holder and accessories are shown in Figure 4.15.

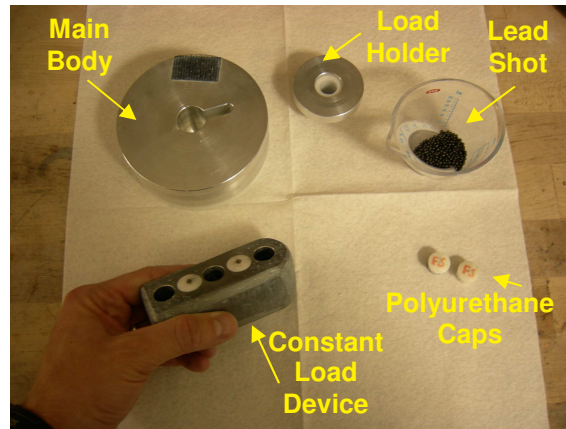


Figure 4.15: Constant load application device

4.4 Experimental Process

For all of the prime experiments, the experimental procedure was the same. At the onset of a polishing run, 500 mL of slurry was measured for pH, density, and temperature, adjustment made if necessary, and the values recorded. All measurements were performed while the slurry was mixed by a magnetic stirring device. The slurry was then transferred to an applicator bottle. The recirculation system was then placed on the polishing machine, and consisted of a catch basin for run-off slurry, flexible tubing fed through a peristaltic pump to draw off the slurry from the basin, and a deposit container placed on a magnetic stirrer to keep the captured slurry thoroughly mixed until reuse. Figure 4.16 shows the complete system.

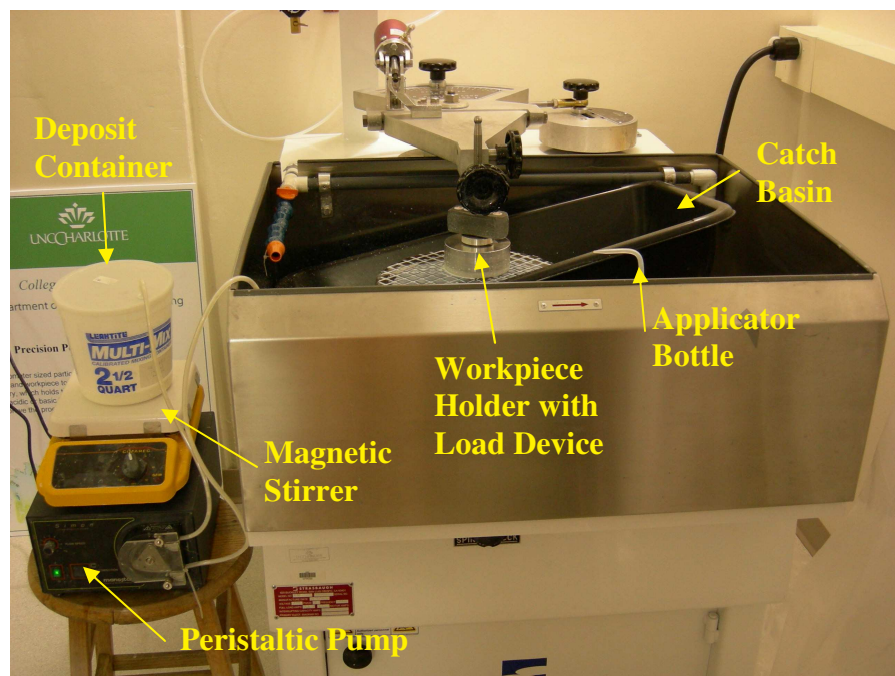


Figure 4.16: Polishing setup with recirculation system

The workpiece material was then mounted into the HDPE holder and the constant load device set for the appropriate material type. The lap was drenched with slurry and the workpiece was moved across the lap surface to distribute the slurry. All components were then mounted in the polisher. The pump, stirrer, and polisher were started and allowed to run for the duration of the experiment. Slurry was applied at the rate of approximately 34 mL/min. Once the run was complete, the entire system was rinsed and cleaned and prepared for the next experiment. The glass was washed, dried, wiped clean with acetone, and stored for measurement.

4.5 Measurement Methodology

For comparison with other technical publications, a full understanding of the measurement methodology is essential. Three separate measurement devices were utilized to characterize the surface finish: 1) Zygo Newview 5000 White Light

Interferometer, 2) Digital Instruments Atomic Force Microscope (AFM), and 3) a Taylor-Hobson Talystep Profilometer. With the interferometer and AFM, two separate scan sizes were utilized and carried through the duration of the experiments.

Two scan lengths were also used for the profilometry, but this was due to a change in measurement strategy after the first experiment set. Initially, it was thought that using a 1 mm scan length would be a useful one because the lateral resolution (approximately 300 nm) was roughly in between that of interferometry and AFM. This method was used for the particle size experiments. However, for the other experiments, it was decided to adopt a measurement strategy used by Leistner [51, 52] in his experiments on Teflon polishing. The scan length was reduced to 200 nm and coupled with the maximum data acquisition rate capable, reduced the lateral resolution to approximately 61 nm, closer to that of the AFM.

The main reason for the switch was because it was found that the generated surfaces were smooth enough to manifest significant problems when measuring with the AFM. It is relatively simple to capture a surface on the AFM when the trace is appreciable. The surfaces presented in this thesis were down in the lower band of the measurement capacity, effectively buried in the noise of the machine for the $1 \mu\text{m}^2$ scan length. As a check, a 750 nm surface from the first experiment set was measured on the higher accuracy AFM located in the Optoelectronics Center at UNC-Charlotte. This AFM was again unable to generate a decent representation of the surface. Thus, the Talystep scan length was adjusted to give information regarding measurements in the higher spatial frequencies. Data was still captured from the AFM, but only the $10 \mu\text{m}^2$ scans were able to show some type of surface.

The captured surface profiles from the Talystep were in raw form and required some manipulation before reporting the results. The data was reduced with the aid of the Internet Based Surface Metrology Algorithm Testing System, provided by the National Institute of Standards and Technology (NIST). Through this program, the data was flattened through subtraction of a 20th order polynomial fit. The waviness (form error) and roughness (surface error) was then calculated and reported.

For completeness, the parameters on the different techniques are summarized in Table 4.3. As the table shows, a wide range of measurement spatial frequencies are captured by this strategy.

Table 4.3: Surface roughness measurement type characteristics

| Measurement Type | Scan Size | FOV | Resolution | Type |
|------------------|--------------------|----------------|--------------------|-------------|
| Interferometer | 2.5X Michelson | 2.82 x 2.11 mm | 4.72 μm | Non-Contact |
| Interferometer | 50X Mirau | 0.14 x 0.11 mm | 640 nm | Non-Contact |
| AFM | 10 μm^2 | - | 39 nm | Contact |
| AFM | 1 μm^2 | - | 3.9 nm | Contact |
| Talystep | 1 mm | - | 300 nm* | Contact |
| Talystep | 200 μm | - | 61 nm* | Contact |

* Value shown is an average value. The exact value depends on the capture rate of the data acquisition system.

The measurements were taken in approximately the same position on the workpiece each time for consistency. All measurements were taken around the center, at approximately 0.5" (12.7 mm), at the 4, 7, and 12 o'clock positions. The non-contact measurements were taken prior to contact methods, to ensure no potential damage was visible in the interferometer results. As described previously, the interferometer was used to measure the step height difference to generate MRR.

Two different surface characterizations are reported, Average Roughness (R_a) and Root Mean Square Roughness (R_q). Both are integrals of a roughness profile, but are generally approximated by the digital forms, shown below [53].

$$R_a = \frac{1}{N} \sum_{j=1}^N |z_j| \quad (4.3)$$

$$R_q = \sqrt{\frac{1}{L} \sum_{j=1}^N z_j^2} \quad (4.4)$$

Average roughness, as Equation 4.3 shows, is simply the average of all data points from a line or area. This parameter is the most common measurement parameter to describe surface finish [54]. The form for R_q is often referred to as standard deviation. This parameter still finds wide application in the optical community, so the values are reported.

4.6 Experimental Sets

The experiment sets were designed to provide a wide range of information with a limited amount of polishing time. As with all experiments, the more experimental runs, the better. However, since the polishing process is slow and the measurement process even slower, the experiments had to maximize the useful data obtained. The main experiment sets are broken up into three basic categories.

- 1) Particle Size Effect on MRR and Surface Finish
- 2) pH Effect on MRR and Surface Finish
- 3) Slurry Density Effect on Material Removal Rates

4.6.1 Particle Size Effect Predictions

The first category will highlight the dominance either mechanical or chemical theories of material removal. As described in section 2.2.1, the Brown/Cook mechanical

model states that MRR should be independent of particle size, but surface roughness should decrease with decreasing particle size. To better understand, imagine a large particle, supporting a certain pressure, indenting into the glass surface. If this large particle were replaced by several smaller ones occupying the same area under the same pressure, the load per particle will decrease. This would mean smaller indentation depths, but there would be more fracture sites. Thus, the model predicts independence of material removal from particle size and concentration.

The chemical model doesn't predict the effects of variable particle size. Since chemical tooth suggests that material is removed in single molecular layers, particle size may play a role simply in the amount of surface area available for bonding. The results of this experiment set should provide some insight.

4.6.2 pH Effect Predictions

The second category focuses on the effect of variable slurry pH, and the subsequent surface charge change, on MRR and surface finish. The mechanical model doesn't predict a change with variable pH and since the particles sizes for these experiments are constant (40 nm), no change should be present within this framework. However, according to the chemical model, a spike in MRR should be seen at pH ~ 7, and falling off on either side of neutral. Changing the pH will adjust the surface charge density on the particle surface and the glass surface. For the abrasive particles, as more positive or negative charges are acquired, the number of available removal sites is decreased. This should trend toward lower MRR. The resulting surface finish is not directly predicted by the chemical model. As seen in section 3.3, researchers have found

varying results on workpiece roughness at all pH levels. The experiments will provide additional data to aid in understanding the chemical model.

Additionally, two types of particle dispersions will be tested (anionic and non-ionic) to see if there is any effect on MRR and surface finish. The polymeric additives themselves are thought not interfere with the particles ability to contact the silica surface, so the removal rates should be consistent between the two. Additionally, there is no direct assumption that surface finish should vary greatly between the two dispersions.

Another point to note is the effect of pH on the silica materials. As pH increases, the workpiece will become more soluble, or softer ([35] after [55]). So, it could be surmised that polishing at higher pH levels could effect higher material removal than at lower pH levels.

4.6.3 Slurry Density Effects

Another important side experiment to determine material removal mechanism is the effects of slurry density on MRR. This experiment set was not exactly an afterthought, rather an ancillary experiment set that could add an additional data point to the determination on which material removal mechanism was dominant. By increasing the slurry density, the particle concentration would also be increased. A mechanical model predicts no effect on material removal with increased particle concentration, while the chemical model suggests increasing MRR with increasing density. This is due to the fact that more abrasive particles mean more surface sites that are available for bonding.

CHAPTER 5: EXPERIMENTAL RESULTS

A key point needs to be understood in reference to the obtained results, which is that the polishing parameters used (i.e. slurry density, concentration, load, relative speed) do not reflect an optimum way to polish a particular glass type. The goal was to keep as many parameters as possible constant, and then knowingly vary one at a time. For instance, to polish quartz, the pressures would have been substantially higher in order to generate larger removal rates. The conditions do not represent the most effective way to polish with the particular slurries either. Nanophase recommends certain pH levels for a particular dispersion, where the abrasive particles are most active, but this research pushed past those set barriers to determine the end effect.

5.1 Particle Size Effect on MRR and Surface Finish

Fused silica and quartz were polished with three abrasive types with variable particle size: CE-6080 (750 nm), CE-6082 (40 nm), and GP-18HD (20 nm). The slurries were mixed at a ratio of 10 parts DI water to 1 part ceria dispersion. The pH of the polishing solutions was not strictly controlled in this experiment set, only annotated. However, the pH stayed in range of the out of box condition (pH ~ 7-8). Both quartz and fused silica were polished with 750, 40, and 20 nm abrasive slurries for 30 minutes each, and repeated three times for a total of 18 polishing runs.

5.1.1 Material Removal Rate Results

Table 5.1 contains the results from the core variable particle size experiments. Preston's coefficient (C_p), as described in section 4.3.1 (Equation 4.2) is also supplied as a measure of the polishing efficiency. Figure 5.1 shows the data graphically.

Judging by these results, it is seen that the initial prediction of MRR staying consistent, within the Brown/Cook mechanical model framework, does not hold. The most striking fact is that the MRR actually decreases dramatically for a respective decrease in particle size. One consideration is that the particle sizes used at present are much smaller than those used in the experiments to validate the mechanical removal model of Brown and Cook. There could be an influencing factor when the mean particle diameters are $\ll 1 \mu\text{m}$. There could also be a definite chemistry aspect at play as well.

Table 5.1: Material removal rate effects of variable particle size

| Glass Type | Particle Size (nm) | Density (g/cm ³) | Temp (°C) | Slurry pH | Removal Rate (nm/hr) | C_p ($\times 10^{-14}$ cm ² /dyn) |
|--------------|--------------------|------------------------------|-----------|-----------|----------------------|---|
| Quartz | 750 | 1.0210 | 22.6 | 7.7 | 16 | 0.138 |
| Quartz | 750 | 1.0209 | 22.5 | 7.48 | 26 | 0.224 |
| Quartz | 750 | 1.0205 | 21.8 | 7.53 | 22 | 0.190 |
| Quartz | 40 | 1.0154 | 22.9 | 7.89 | 4 | 0.035 |
| Quartz | 40 | 1.0152 | 23.8 | 7.6 | 4 | 0.035 |
| Quartz | 40 | 1.0156 | 23.3 | 7.5 | 2 | 0.017 |
| Quartz | 20 | 1.0137 | 23.1 | 7.93 | ~1 | 0.009 |
| Quartz | 20 | 1.0140 | 23.5 | 7.76 | ~1 | 0.009 |
| Quartz | 20 | 1.0142 | 23.4 | 7.67 | ~2 | 0.017 |
| Fused Silica | 750 | 1.0210 | 22.6 | 7.7 | 284 | 2.442 |
| Fused Silica | 750 | 1.0209 | 22.5 | 7.48 | 282 | 2.425 |
| Fused Silica | 750 | 1.0205 | 21.8 | 7.53 | 288 | 2.476 |
| Fused Silica | 40 | 1.0154 | 22.9 | 7.89 | 30 | 0.258 |
| Fused Silica | 40 | 1.0152 | 23.8 | 7.6 | 22 | 0.189 |
| Fused Silica | 40 | 1.0156 | 23.3 | 7.5 | 20 | 0.172 |
| Fused Silica | 20 | 1.0137 | 23.1 | 7.93 | 12 | 0.103 |
| Fused Silica | 20 | 1.0140 | 23.5 | 7.76 | 14 | 0.120 |
| Fused Silica | 20 | 1.0142 | 23.4 | 7.67 | 10 | 0.086 |

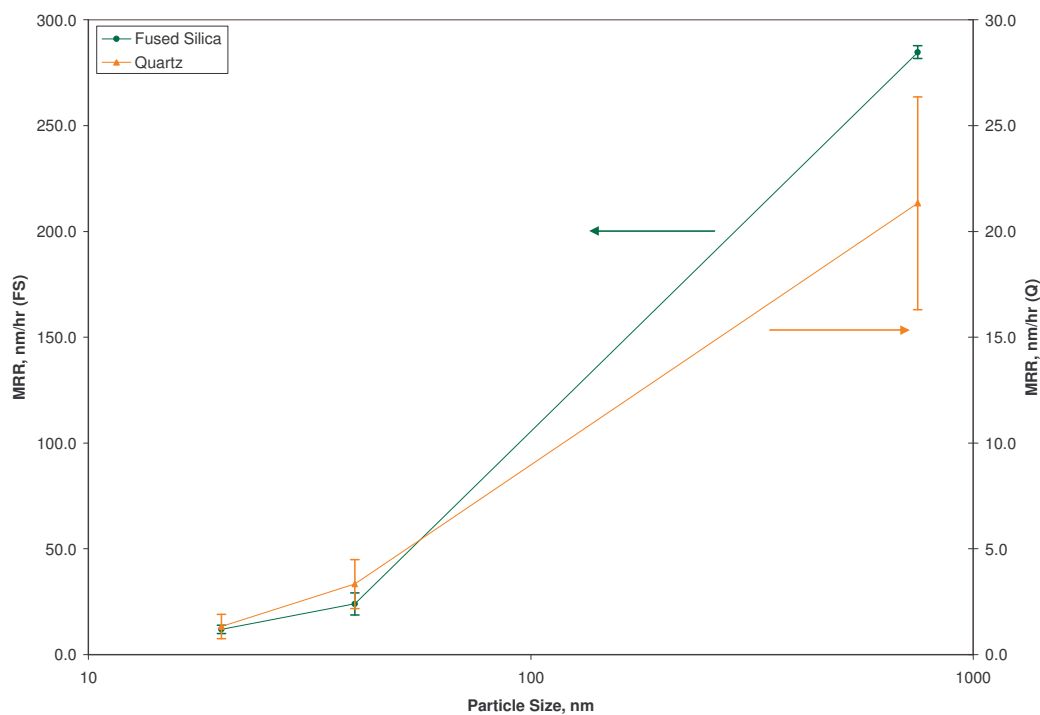


Figure 5.1: MRR versus particle size for quartz and fused silica

When the data are normalized, the results can be plotted on a log-log chart, with MRR on the ordinate and particle size on the abscissa, as shown in Figure 5.2. The relationship is linear for both, raising an interest in being able to predict removal rates based on particle size. However, this is only a single set of data and many more experiments should be conducted before coming to a definite conclusion. It does, however, provide an interesting subject of discussion.

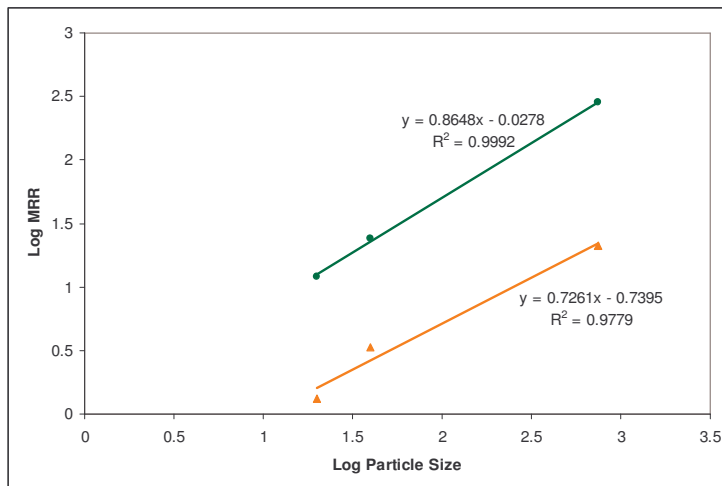


Figure 5.2: Log-Log plot of MRR versus particle size

5.1.2 Surface Finish Results

The next review of the data must look at the resulting surface finish. Table 5.2 and Figure 5.3 show the surface finish results for the variable particle size experiments. It is readily evident that the surface finish did not change drastically with particle size. An important point to note is the questionability of the $1 \mu\text{m}^2$ AFM scans. As discussed in section 4.5, the surfaces were smooth enough to become buried in the noise of the machine. The results are presented here for completeness, but the reader is encouraged to take caution when interpreting these results. Also, the $1 \mu\text{m}^2$ AFM scan of fused silica polished with 20 nm particles is suspect for another reason. The slightly higher R_a are thought to have resulted measurement probe shear. Initially, the values were taken as accepted, but after comparison of all the results, it appeared to be out of range.

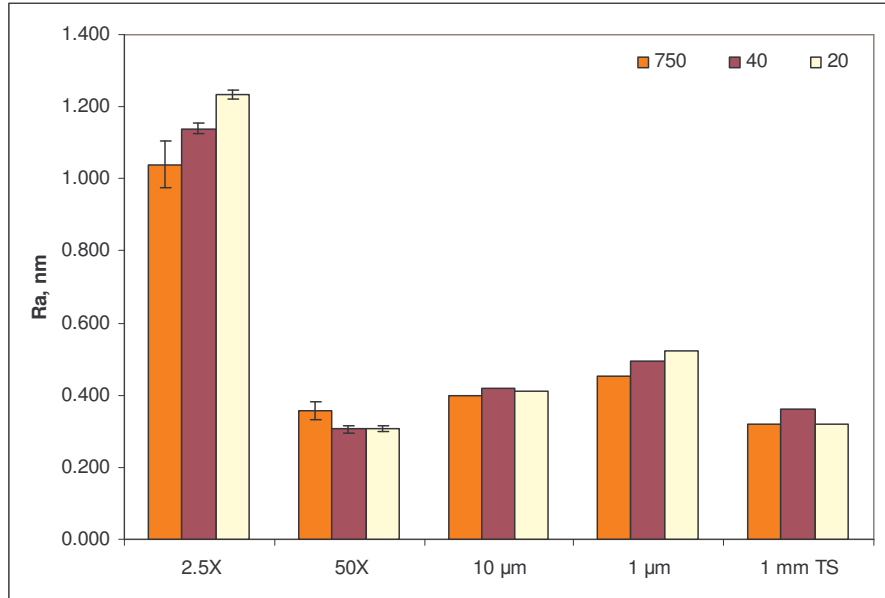
A point should be noted on the contact measurements, namely the AFM and Talystep measurements. As described above, the surface roughness did not drastically change with the respective experiments. This was especially true on the higher spatial frequency contact measurements. Thus, it was decided to only take representative

measurements with respect to a certain variable change experiment (i.e. representative measurement with 750, 40, and 20 nm particles). This is why scatter bars are not present on the graph in Figure 5.3. These values are shown as an average of three measurements after the final experiment in the particular set.

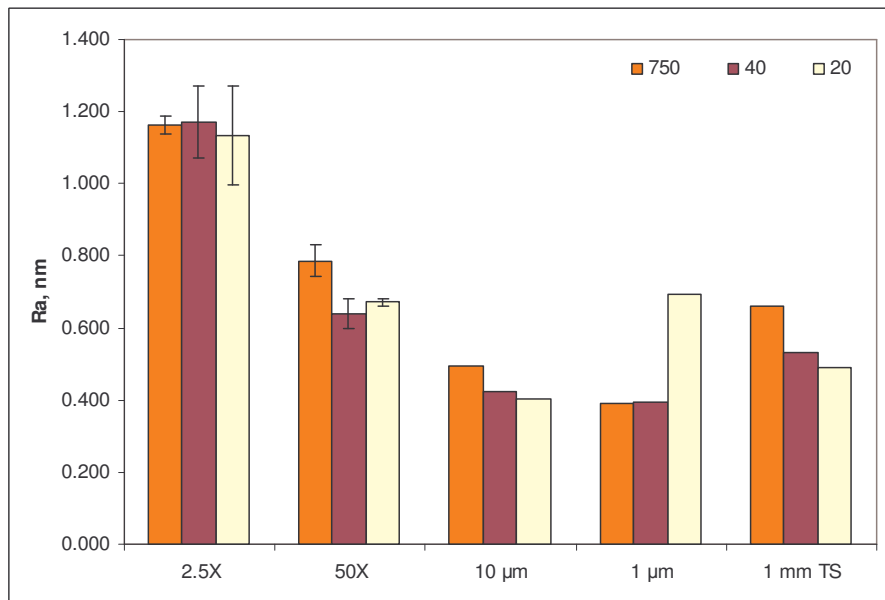
The surface finish results go against a purely mechanical removal model, which states roughness should decrease with particle size. The results seem to show that chemistry could be playing an active role in the final surface, perhaps through redeposition of silica on the glass surface.

Table 5.2: Surface finish effects of variable particle size

| Glass Type | Particle Size (nm) | White Light Interferometer Average Measurements (nm) | | | | Atomic Force Microscope Average Measurements (nm) | | | | Talystep - 1 mm Scan Average Measurements (nm) Roughness and Waviness | | | |
|--------------|--------------------|---|-------|------------|-------|--|-------|-------------------|-------|---|------|------|------|
| | | 2.5X Mich | | 50X Mireau | | 10 μm^2 | | 1 μm^2 | | Ra | W | Rq | W |
| Quartz | 750 | 1.033 | 1.541 | 0.381 | 0.497 | 0.397 | 0.502 | 0.454 | 0.586 | 0.32 | 0.17 | 0.41 | 0.22 |
| Quartz | 750 | 0.981 | 1.245 | 0.363 | 0.488 | | | | | | | | |
| Quartz | 750 | 1.107 | 1.390 | 0.332 | 0.425 | | | | | | | | |
| Quartz | 40 | 1.150 | 1.434 | 0.295 | 0.371 | 0.419 | 0.537 | 0.496 | 0.640 | 0.36 | 0.23 | 0.45 | 0.27 |
| Quartz | 40 | 1.145 | 1.438 | 0.317 | 0.398 | | | | | | | | |
| Quartz | 40 | 1.124 | 1.425 | 0.307 | 0.402 | | | | | | | | |
| Quartz | 20 | 1.248 | 1.564 | 0.303 | 0.381 | 0.411 | 0.529 | 0.525 | 0.682 | 0.32 | 0.09 | 0.4 | 0.11 |
| Quartz | 20 | 1.226 | 1.567 | 0.317 | 0.417 | | | | | | | | |
| Quartz | 20 | 1.230 | 1.561 | 0.303 | 0.381 | | | | | | | | |
| Fused Silica | 750 | 1.188 | 1.499 | 0.831 | 1.090 | 0.492 | 0.638 | 0.392 | 0.495 | 0.66 | 0.22 | 0.89 | 0.27 |
| Fused Silica | 750 | 1.139 | 1.448 | 0.745 | 1.050 | | | | | | | | |
| Fused Silica | 750 | 1.160 | 1.519 | 0.785 | 1.021 | | | | | | | | |
| Fused Silica | 40 | 1.284 | 1.622 | 0.630 | 0.820 | 0.423 | 0.541 | 0.395 | 0.493 | 0.53 | 0.19 | 0.80 | 0.23 |
| Fused Silica | 40 | 1.093 | 1.413 | 0.607 | 0.804 | | | | | | | | |
| Fused Silica | 40 | 1.138 | 1.445 | 0.687 | 0.866 | | | | | | | | |
| Fused Silica | 20 | 1.195 | 1.504 | 0.680 | 0.882 | 0.404 | 0.541 | 0.693 | 0.893 | 0.49 | 0.13 | 0.71 | 0.16 |
| Fused Silica | 20 | 1.232 | 1.544 | 0.659 | 0.880 | | | | | | | | |
| Fused Silica | 20 | 0.978 | 1.239 | 0.676 | 0.910 | | | | | | | | |



(a)



(b)

Figure 5.3: Comparison of surface finish measurements with (a) quartz and (b) fused silica, as a function of particle size. Polishing order (750 nm à 40 nm à 20 nm)

5.2 pH Effect on MRR and Surface Finish

Silica material polishing was conducted with CE-6082 (40 nm anionic) and CE-6086 (40 nm non-ionic) slurries at three different pH levels (4, 7, 10). Both silica workpiece types were run twice at each pH value (4, 7, and 10) for a total of 12 experiments with CE-6082. Fused silica was also polished twice at each pH value (4, 7, 10) for a total of 6 experiments with CE-6086. Only fused silica was used in this set based on the low amount of material removal found for quartz in the particle size and pH experiments with CE-6082. This was considered sufficient since the variable parameters studied up to this point didn't have much effect on the material removal of quartz, and a better representation of the effects will be seen with fused silica.

5.2.1 Material Removal Rate Results with Anionic Dispersion

Table 5.3 contains the results from the variable pH experiments with an anionic dispersion. Again, C_p is provided and Figure 5.4 presents the graphical data.

Table 5.3: Material Removal Rate Effects of Variable pH (anionic dispersion)

| Glass Type | Slurry pH | Particle Size (nm) | Density (g/cm ³) | Temp (°C) | Removal Rate (nm/hr) | C_p (x 10 ⁻¹⁴ cm ² /dyn) |
|--------------|-----------|--------------------|------------------------------|-----------|----------------------|--|
| Quartz | 4.01 | 40 | 1.0155 | 23.6 | <1 | 0.009 |
| Quartz | 3.99 | 40 | 1.0155 | 23.8 | 2 | 0.017 |
| Quartz | 6.98 | 40 | 1.0154 | 23.5 | 4 | 0.035 |
| Quartz | 6.98 | 40 | 1.0159 | 23.9 | 4 | 0.035 |
| Quartz | 10.02 | 40 | 1.0155 | 23.3 | <1 | 0.009 |
| Quartz | 10.02 | 40 | 1.0155 | 23.9 | 1 | 0.009 |
| Fused Silica | 4.01 | 40 | 1.0155 | 23.6 | 35 | 0.301 |
| Fused Silica | 3.99 | 40 | 1.0155 | 23.8 | 42 | 0.361 |
| Fused Silica | 6.98 | 40 | 1.0159 | 23.9 | 235 | 2.021 |
| Fused Silica | 6.99 | 40 | 1.0162 | 24 | 554 | 4.764 |
| Fused Silica | 10.02 | 40 | 1.0155 | 23.3 | 245 | 2.107 |
| Fused Silica | 10.02 | 40 | 1.0155 | 23.4 | 315 | 2.709 |

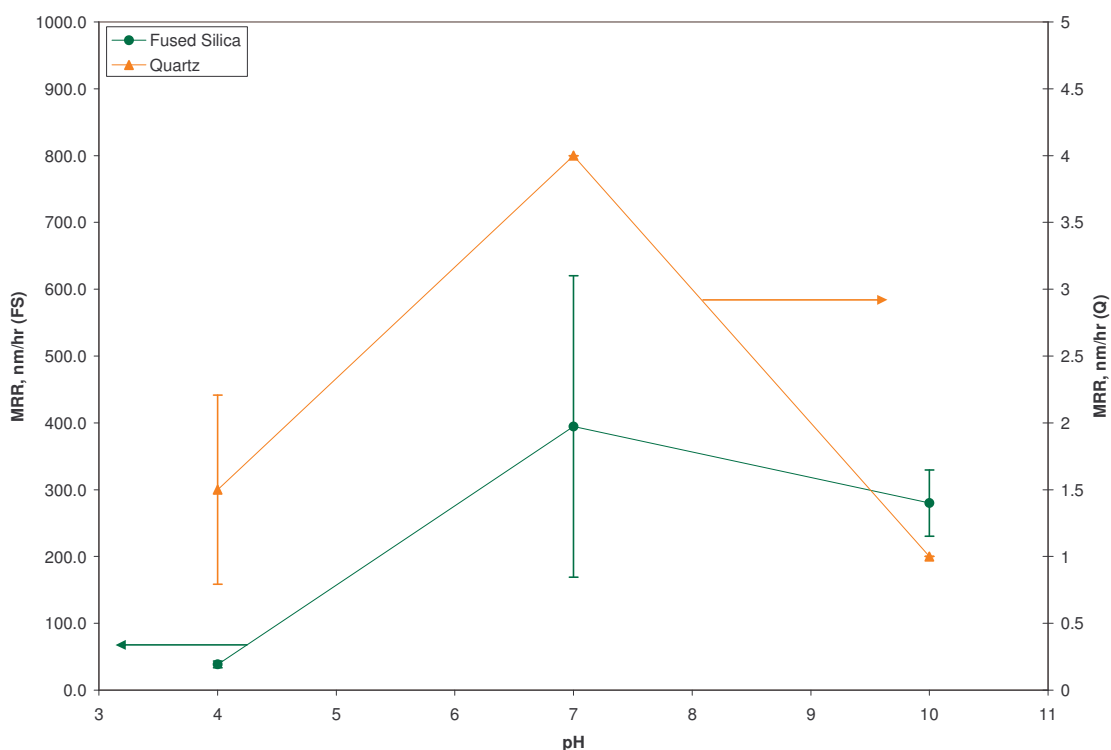
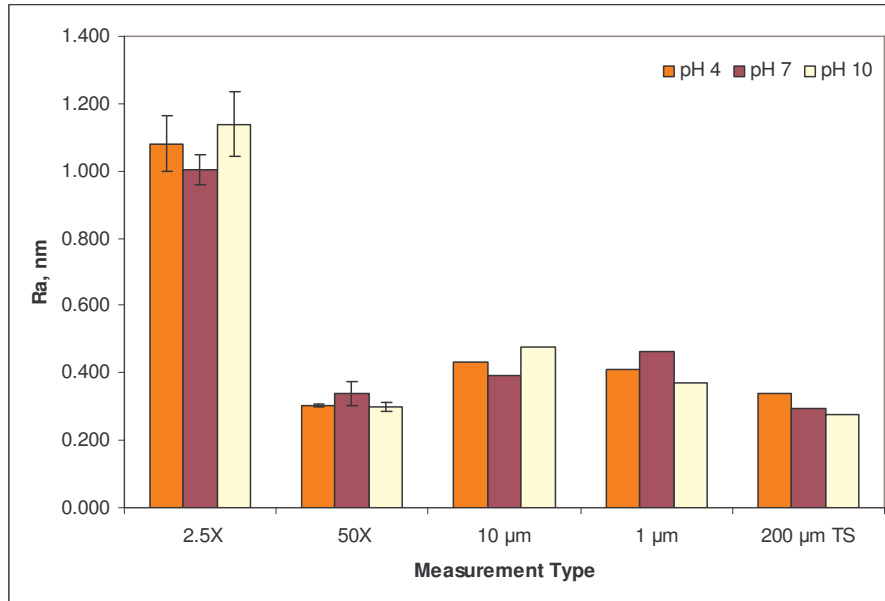
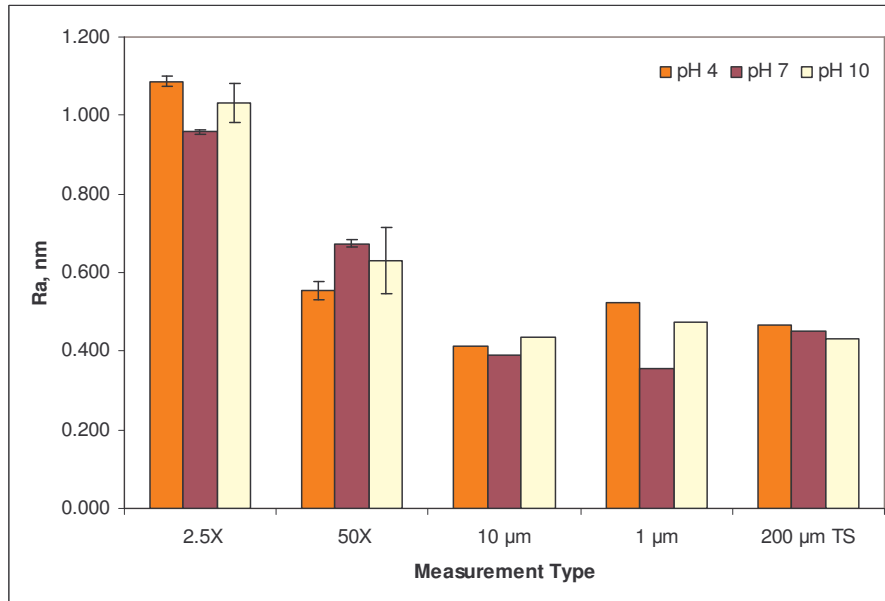


Figure 5.4: MRR versus pH for quartz and fused silica with anionic dispersion

Under the auspices of the mechanical model, the MRR should not have been affected greatly by the underlying chemistry. However, the results definitely show that chemistry is playing a role in material removal. There is a notable spike in MRR at pH 7, as expected. Since ceria has a pzc of pH 6.8, this pH is very close to where the chemical tooth model proposes that material removal will be the maximum. At the acidic solution level, the MRR drops significantly. This is most likely due to the fact that the particle surface has an acquired excess positive charge, thus becoming a hydrogen proton donator to the glass surface and drastically reducing the amount of bonding. At the basic solution level, MRR is lower, but within the scatter bars of the neutral pH solution. The relatively substantial amount of removal at this level could be attributed to the glass becoming more soluble (i.e. softer) in the increasingly corrosive environment.



(a)



(b)

Figure 5.5: Comparison of surface finish measurements with (a) quartz and (b) fused silica, as a function of pH (anionic dispersion). Polishing Order (pH 7 à pH 10 à pH 4)

5.2.3 Material Removal Rate Results with Non-Ionic Dispersion

Table 5.5 contains the results from the core variable pH experiments with the non-ionic dispersion slurry. C_p is provided and Figure 5.6 shows the same data in a graphical representation, where the effect of pH is more readily seen.

Table 5.5: Material Removal Rate Effects of Variable pH (non-ionic dispersion)

| Glass Type | Slurry pH | Particle Size (nm) | Density (g/cm ³) | Temp (°C) | Removal Rate (nm/hr) | C_p ($\times 10^{-14}$ cm ² /dyn) |
|--------------|-----------|--------------------|------------------------------|-----------|----------------------|---|
| Fused Silica | 3.99 | 40 | 1.0155 | 23.7 | 53 | 0.456 |
| Fused Silica | 4.02 | 40 | 1.0155 | 23.8 | 153 | 1.316 |
| Fused Silica | 7.01 | 40 | 1.0155 | 23.8 | 256 | 2.201 |
| Fused Silica | 7.02 | 40 | 1.0155 | 23.9 | 415 | 3.568 |
| Fused Silica | 10 | 40 | 1.0155 | 23.6 | 300 | 2.580 |
| Fused Silica | 10.04 | 40 | 1.0155 | 24.2 | 359 | 3.087 |

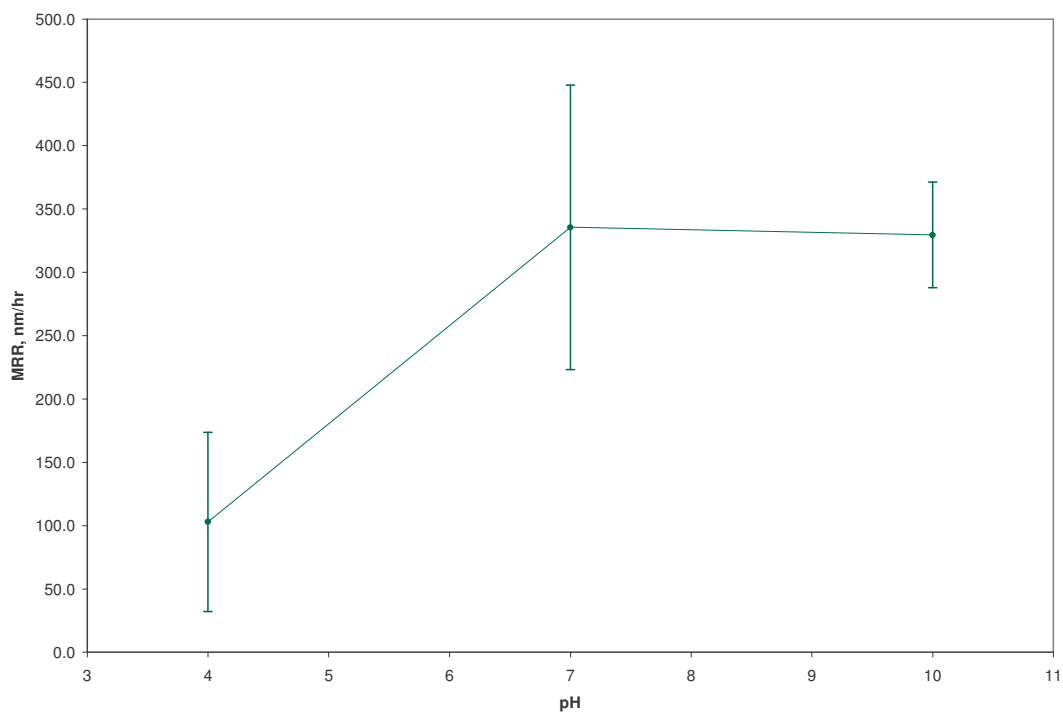


Figure 5.6: MRR versus pH for fused silica with non-ionic dispersion

As previously noted, the mechanical model predicts no change in MRR with varying pH. As seen, the pH did affect the MRR, with the same trends noted for the anionic slurries, although they were, on average, slightly lower.

5.2.4 Surface Finish Results for Non-Ionic Dispersion

Table 5.6 and Figure 5.7 contain the review on resulting surface finish after polishing with the different pH solutions with the non-ionic slurry. It is seen that the surface roughness did not change substantially except with the 2.5X interferometer scan.

Table 5.6: Surface finish effects of variable pH (non-ionic dispersion)

| Glass Type | Slurry pH | White Light Interferometer Average Measurements (nm) | | | | Atomic Force Microscope Average Measurements (nm) | | | | Talystep - 1 mm Scan Average Measurements (nm) Roughness and Waviness | | | |
|--------------|-----------|---|-------|------------|-------|--|-------|-------------------|-------|---|-------|-------|-------|
| | | 2.5X Mich | | 50X Mireau | | 10 μm^2 | | 1 μm^2 | | Ra | W | Rq | W |
| | | Ra | Rq | Ra | Rq | Ra | Rq | Ra | Rq | | | | |
| Fused Silica | 3.99 | 1.097 | 1.442 | 0.732 | 0.922 | 0.397 | 0.516 | 0.402 | 0.524 | 0.397 | 0.000 | 0.520 | 0.000 |
| Fused Silica | 4.02 | 1.212 | 1.583 | 0.644 | 0.809 | | | | | | | | |
| Fused Silica | 7.01 | 1.654 | 2.131 | 0.720 | 0.920 | 0.407 | 0.526 | 0.365 | 0.461 | 0.443 | 0.000 | 0.627 | 0.000 |
| Fused Silica | 7.02 | 1.498 | 1.901 | 0.762 | 0.973 | | | | | | | | |
| Fused Silica | 10 | 1.860 | 2.283 | 0.719 | 0.906 | 0.374 | 0.478 | 0.362 | 0.458 | 0.513 | 0.000 | 0.713 | 0.000 |
| Fused Silica | 10.04 | 2.465 | 3.147 | 0.698 | 0.878 | | | | | | | | |

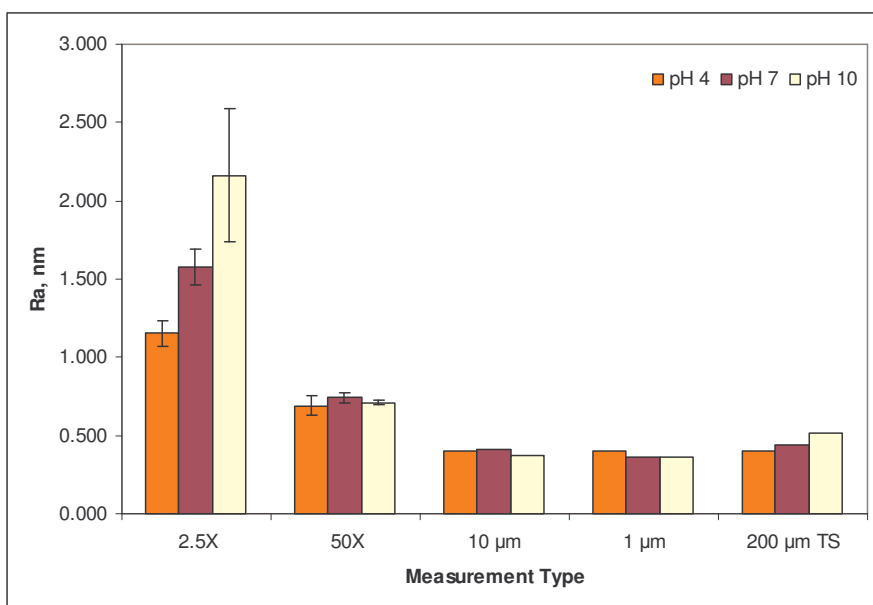


Figure 5.7: Comparison of surface finish measurements with fused silica as a function of pH with a non-ionic dispersion. Polishing Order (pH 7 à pH 10 à pH 4)

The roughness increase is attributed to microscratching and pitting on the glass surface. It is evident on the 2.5X interferometer scan, since the field of view is the largest of the measurement types (2.82 x 2.11 mm). The smaller FOV scans were thus in between the surface features. Figure 5.8 shows a comparison between two scans from experiment sets 1 and 2. It should be noted that the measurements were made in approximately the same area.

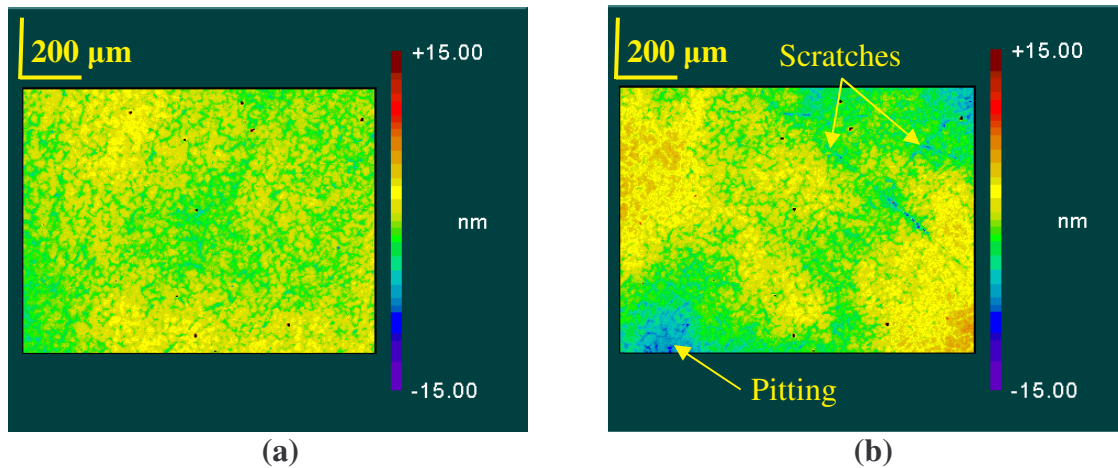


Figure 5.8: Comparison of fused silica surface from (a) anionic dispersion set ($R_a = 0.955$ nm) and (b) non-ionic dispersion set ($R_a = 1.726$), both conducted at pH=7

5.3 Slurry Density Effect

While the density of the slurry could be controlled, there was some interest in understanding how variation in density could affect material removal, since density is an indirect measure of the number of available particles for polishing. The polishing was performed on pitch with CE-6082 (40 nm) slurry kept at a constant pH of 7. The polishing pressure and relative velocity were kept constant at 39.8 gf/cm^2 (equivalent to applying a 4 lb dead weight load) and 9.4 cm/s , respectively. The density was varied from 1.005 – 1.035 g/cm^3 . Fused silica was the polishing workpiece used, and two 1-hour runs were performed at each of four densities for a total of 8 experiments.

The results of the experiments are provided as averaged values in Table 5.7 and shown graphically in Figure 5.9 (with standard deviations shown as error bars).

Table 5.7: Material Removal Rate Effects of Variable Slurry Density

| Glass Type | Density (g/cm ³) | Slurry pH | Temp (°C) | Removal Rate (nm/hr) | C _p (x 10 ⁻¹⁴ cm ² /dyn) |
|--------------|------------------------------|-----------|-----------|----------------------|---|
| Fused Silica | 1.005 | 7.01 | 23.5 | 145 | 1.247 |
| Fused Silica | 1.005 | 7.02 | 23.9 | 122 | 1.049 |
| Fused Silica | 1.015 | 7 | 24 | 135 | 1.161 |
| Fused Silica | 1.015 | 7.02 | 23.5 | 138 | 1.187 |
| Fused Silica | 1.025 | 7 | 24 | 149 | 1.281 |
| Fused Silica | 1.025 | 7.01 | 24.1 | 161 | 1.384 |
| Fused Silica | 1.035 | 7.01 | 23.9 | 188 | 1.617 |
| Fused Silica | 1.035 | 7.02 | 24 | 182 | 1.565 |

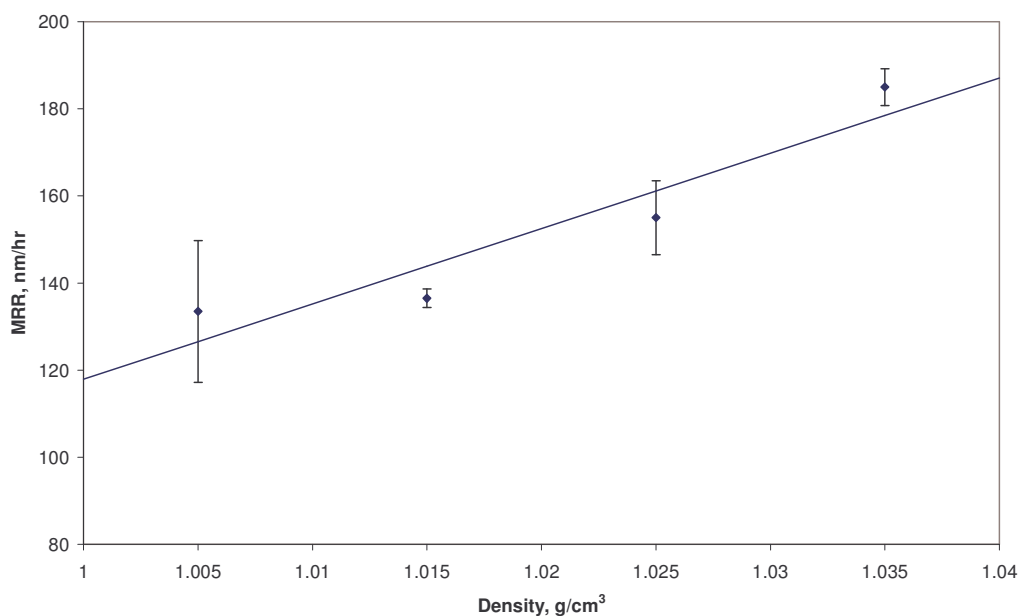


Figure 5.9: Graphical representation of the variable density experiments

It is readily evident that the removal rates showed an increasing trend with increasing density of the slurry. With the assumption that there were indeed more abrasive particles present with increasing slurry density, material removal by the

mechanical model is not supported since it is theoretically unaffected by the particle concentration. From a chemical standpoint, more particles mean more surface sites are available to react on the glass surface, offering evidence for chemical theory.

It is also worthwhile to investigate the theoretical increase in the number of abrasive particles available for polishing. This value can be predicted by utilizing a modeling scheme developed by Dr. Ed Paul from Stockton College [25, 56]. The model is based on separate examination of the liquid and solid phase of the solution and assuming a spherical particle. The equations used are shown below:

$$\%A = \frac{\rho_A(\rho - \rho_f)}{\rho(\rho_A - \rho_f)} \cdot 100 \quad [A] = \frac{6}{\pi d_A^3} \left[\frac{\%A}{(1 - \rho_A / \rho_f) \cdot \%A + 100(\rho_A / \rho_f)} \right] \quad (5.1)$$

- $\%A$ $\hat{=}$ the weight percentage of abrasive present
- ρ $\hat{=}$ density of system
- ρ_A $\hat{=}$ density of abrasive
- ρ_f $\hat{=}$ density of fluid (water)
- d_A $\hat{=}$ diameter of abrasive particle
- $[A]$ $\hat{=}$ number of abrasive particles

By applying these equations to the 40 nm particle, the values in Table 5.8 are found. As a check, it is noted that an 18 wt% ceria slurry, with 40 nm particles, diluted 10:1 with water has a measured density of 1.0155 g/cm³. After dilution, the weight percent of the slurry should be around 1.8 wt%. When the value of %A is calculated with this density, a value of 1.796% is found, in close agreement with the expected value. Thus, the model seems to accurately predict an increase in the amount of abrasive particles available for polishing.

Table 5.8: Theoretical calculations of variable density slurries

| Particle Size (nm) | Slurry Density (g/cm ³) | %A | [A] |
|--------------------|-------------------------------------|-------|-------------|
| 40 | 1.005 | 0.585 | 2.63758E+13 |
| 40 | 1.015 | 1.739 | 7.91273E+13 |
| 40 | 1.025 | 2.870 | 1.31879E+14 |
| 40 | 1.035 | 3.979 | 1.8463E+14 |

5.4 Additional Comments on Experimental Results

Several topics of discussion are also needed to interpret the results given. The first is a comparison between quartz and fused silica in each experimental set. From the results, it is seen that the quartz was barely polishing while the fused silica had appreciable material removal, under these conditions. The reason is most likely the underlying bulk structure of the materials. Fused silica is an amorphous structure, characterized by unequal bond lengths between silica tetrahedra, and as a result there will be some amount of strain between these bonds. This makes the material more likely to be affected by a polishing operation. The quartz has a definite crystalline structure with no strained bonds. This makes the material less susceptible to reaction with abrasive particles. These facts tended towards higher removal rates and a surface with more valleys for fused silica.

A statistical analysis was performed on the Talystep roughness data of fused silica and quartz and the skewness of the line profiles was calculated. Skewness, R_{sk} , is a parameter that gives indications of the amount of peaks/valleys present on a surface. A positive R_{sk} corresponds to a predominantly peaked surface, and negative R_{sk} corresponds to a surface with more valleys. The results showed that fused silica was typically

negatively skewed and quartz was at near zero skew values. This trend was evident in all of the experimental sets. Representative 50X interferometer pictures shows several typically generated surfaces.

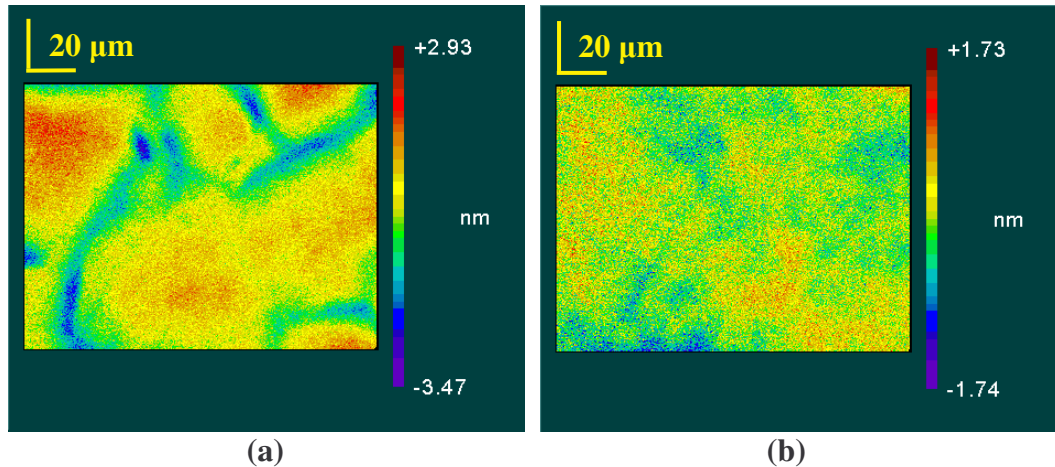


Figure 5.10: Representative 50X interferometer pictures of (a) fused silica ($R_a = 0.600$ nm) and (b) quartz ($R_a = 0.296$ nm). Both polished with 40 nm anionic dispersion at pH = 7.

An additional comment needed is in regards to the removal rate comparison between the particle size and pH experiments. As described in section 4.1.1, the small abrasive pitch tool was run in for 12 hours before experimentation began. The tool then received 6 hours of polishing in experiment set 1, 3 hours with a 40 nm abrasive slurry and 3 hours with a 20 nm abrasive slurry. The next polishing performed was in the pH experiments recorded in this section, which were all done on the small abrasive pitch tool. However, the MRR increased significantly for fused silica during these experiments.

Several considerations were made as to how the MRR could increase. The rate of removal should be linear over the polishing time, but a check was warranted since polishing time for experiment set 1 was 30 minutes and 1 hour for experiment set 2.

After completion of all the experiments in this thesis, several polishing runs were performed under the same conditions as the 40 nm particle trials in experiment set 1 (i.e. same density and out-of-box pH). The runs were for 30 minutes each and the MRR was 178 nm/hr (89 nm/30 min) and 176 nm/hr (88 nm/30 min). These results were consistent and higher than the values found in experiment set 1, indicating a more efficient tool. An explanation could be proposed by noting the fact that MRR didn't increase until the pitch tool was loaded with the 20 nm abrasive slurries. When the polishing began with 40 nm abrasive slurries in experiment set 2, the embedded 20 nm particles must have been at work. Regardless of the reason why, the pitch tool obviously became more efficient. Thus, a direct comparison between particle size and pH experiments should not be made. Rather, only the relative results should be compared within each experiment set.

CHAPTER 6: DISCUSSION

As is normally the case for polishing experimentation, the results presented in this thesis provide a fruitful ground for discussion. The results provide some hard evidence, as well as raise new issues with respect to the material removal theories. The evidence will be discussed, as well as other influencing factors seen during the course of experimentation.

6.1 Discussion on Removal Mechanism Theories

The experiments discussed in Section 4.6 and the results highlighted in Chapter 5 provide a great deal of information and justification for the chemical model of material removal, versus the Brown/Cook model for mechanical abrasion. Each of the variables contained in the experiment sets provide some amount of justification either for or against these two models.

6.1.1 Mechanical Removal Theory

Particle Size

The Brown/Cook mechanical model proposes that MRR should be independent of particle size. However, the results show that MRR decreased drastically for a respective large decrease in mean particle diameter. For both quartz and fused silica, an order of magnitude decrease in particle size equated to an order of magnitude lower removal rates. Additionally, the mechanical model states that surface roughness should decrease with

decreasing particle size. The mechanical wear is through the process of scratching the glass surface to effect material removal. Larger particles correlate with larger scratches, and smaller particles with smaller scratches, with equivalent loading. Again, the model fails to hold since the surface finish did not drastically change with particle size.

It is also worthwhile to mention that the papers proposing the Brown/Cook mechanical model [31, 33] used particles that were larger (on the order of 1 μm) than the nanoparticles used in this work. The nanoparticles may be small enough to negate some of the underlying assumptions made in the development of the Brown/Cook model. In other words, there may be a limit where mechanical models predict accurately, and below this value the chemistry becomes a more prevalent factor. Further investigation into the mechanical aspects of these small particles (i.e. $\ll 1 \mu\text{m}$) will be the subject of a future work on theoretical modeling, highlighted in Chapter 7.

Polishing Dispersion pH

The mechanical theory does not account for chemistry changes, as in modification of the polishing solution pH, and thus predicts no change in MRR and surface finish with varying solution pH. However, it was seen that the maximum removal was at pH 7, with intermediate values at basic solution levels and lowest at acidic solution levels. Again, the mechanical model does not hold and indicates chemistry is playing a vital role.

Particle Concentration

Particle concentration is also suspected of having no effect on MRR according to the mechanical theory. By changing the density, it was assumed that the particle concentration increased, which is a valid assumption. As shown in section 5.3, there is

some mathematical justification to this statement. Increasing particle concentration was shown to have a respective increase in MRR, which goes against a pure mechanical removal theory.

6.1.2 Chemical Removal Theory

Particle Size

The chemical theory offers no hypothesis of MRR or surface finish effects with variable particle size. It was noticed, however, that the surface roughness remained consistent regardless of particle size. An argument can be made that this supports chemical effects, since the chemical tooth theory suggests that material is pulled away from the silica surface by monolayers at a time. Thus, regardless of size, the particles will only pluck material based on the amount of surface area in contact with the silica.

The model also does not explain why the MRR decreased with decreasing particle size. A thought is that there is a change in the amount of particle surface area bonding with the silica. Modeling a spherical ceria particle on a flat plate is one way to look at this assumption. Ceria is actually softer (~ 6 on the Mohs scale) than the silica (7 on the Mohs scale). Thus, when a force is applied, there will be some amount of compliance associated with the particle. The force per particle, and thus the radius of the contact circle will change with a change in particle size, and with other factors such as particle concentration. This idea is shown schematically in Figure 6.1, and will be a topic of future work on theoretical modeling, highlighted in Chapter 7.

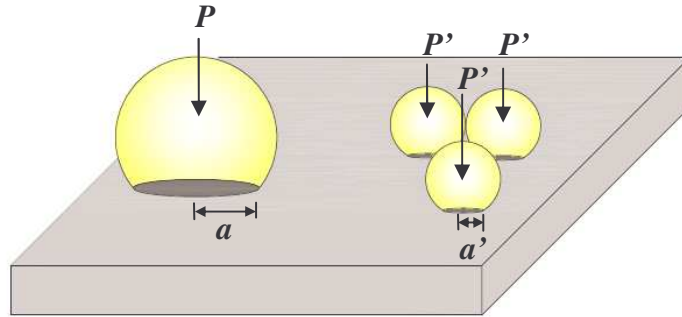


Figure 6.1: Indentation of a sphere on a flat plate with (a) particle with a nominal load P and contact radius a and (b) smaller particles occupying a similar area with a distributed load P' and contact radii a'

Polishing Dispersion pH

Reviewing the results shown in Section 5.2, it is readily seen that solution pH plays an active role in MRR. The maximum MRR was achieved at pH of 7, with intermediate values at basic levels and low values at acidic levels. This is exactly what was expected with the chemical removal model, so it did not come as a surprise. What was interesting however, is the fact that the removal rates were comparable at pH 10 with those results from pH 7. As indicated by the work of Suphantharida and Osseo-Asare [46], and explained in section 3.3, experimental results have shown that maximum material removal could occur closer to pH 9 where silicate adsorption onto ceria is maximum, versus the chemical tooth maximum prediction of pH 6.8. This likely has to do with glass solubility in corrosive basic solutions during the polishing process. This subject also has potential for study, and will be a topic for future work on surface chemistry effects, highlighted in Chapter 7.

Particle Concentration

The particle concentration experiments showed that MRR increased with more particles. This fact also supports chemical theory in that more abrasive particles mean more bonding sites for material to be plucked from the silica surface.

6.1.3 Realities of Polishing

The results provided may appear as an attempt to completely shoot down the Brown/Cook model, but this is definitely not the case. As discussed in the motivation (Section 3.4), the goal was to highlight the dominance of either the Brown/Cook mechanical or chemical removal mechanisms.

In reality, the polishing process is, as described in Chapter 3, a process of both chemical and mechanical actions. It is impossible to physically separate the two when discussing chemically active particles and glass. It is the dominance of either portion that is really the question at hand. Mechanical action of physically placing particles in contact with the silica surface and then removing them is a necessary part of polishing. The chemical bonding between the particle and silica is also apparently necessary. The experimental results have shown that, under the conditions presented, that the chemical tooth seems to be the dominant removal mechanism in ceria-silica polishing. The MRR is affected in a manner depicted by the chemical tooth theory (variable pH), and the surface finish is also supported by the model in that it predicts generation of by products (in the form of silicic acid) that can redeposit on the silica surface (see Equation 3.4 in Sec. 3.1.2) and produce smooth surfaces.

6.2 Slurry Dispersion Effects

It is worthwhile to discuss the assumption made in Sections 3.2.3 and 4.6.2 that the polymeric additives in the ceria dispersions would not affect the particle interaction with the silica workpiece. Indeed, this seems to be the case since appreciable amounts of material was removed. The thought on why these polymer chains don't interfere is that they are pushed out of the way when a particle is loaded under pressure, thus allowing the ceria surface to come in contact with the silica material. This would effectively explain, from a chemical viewpoint, why these particles are able to effect material removal, since they are able to bond to the silica surface. Figure 6.2 shows a schematic view of this interpretation.

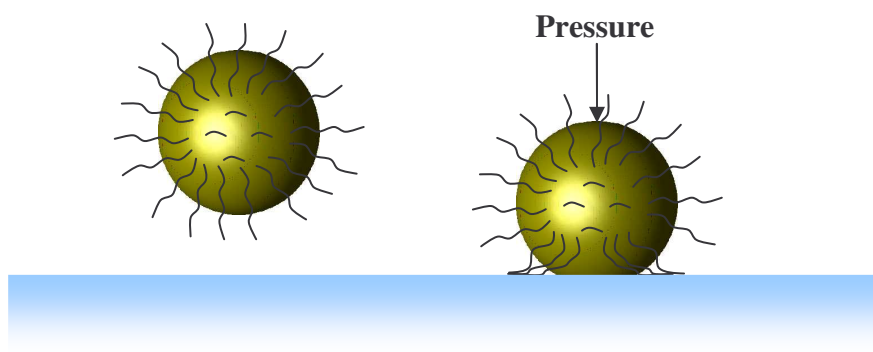


Figure 6.2: Abrasive particle with polymeric coating interaction with silica

A comparison of the results between polishing fused silica with anionic and non-ionic dispersion is given in Figure 6.3. As is readily seen, the MRR did not seem affected by the two different types of colloidal stability methods. The obvious exception to this statement is that the anionic dispersion seems more sensitive at neutral pH levels, since there was a greater variation in the amount of material removed. Another interesting trend noticed is in the surface finish. With the anionic dispersion, the surface roughness

was least at pH 7, and comparable at acidic and basic conditions. With the non-ionic, the roughness decreased with decreasing pH. The anionic dispersion matches trends with the work of Cumbo, et al [47], and the non-ionic dispersion matches trends with the work of Tesar, et al [48], both of which were described in Section 3.3. The exception is that the latter did not run polishing tests at alkaline levels. This is interesting in that the anionic and non-ionic results match up with the Cumbo and Tesar results, respectively, but not with each other. This tends to indicate that the dispersion is having an effect on the surface finish, but exactly what that effect is remains unclear. Additional work is needed to explore the effects.

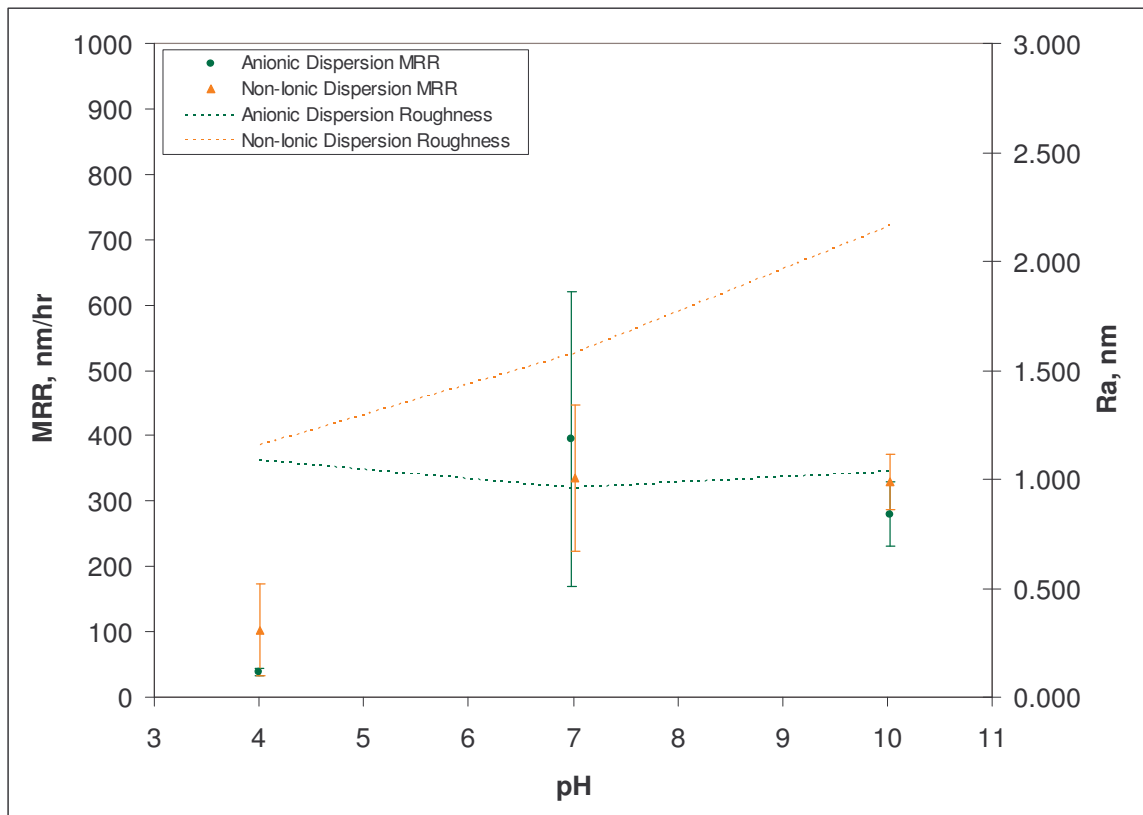


Figure 6.3: Comparison of pH experiments with anionic and non-ionic dispersion slurries

CHAPTER 7: CONCLUSIONS AND FUTURE WORK

The procedures and results contained in this thesis provide strong supporting evidence that chemistry plays a vital role in the polishing of silica materials with metal oxide abrasives, namely ceria. Several novel methods were also presented, as highlighted in the ancillary conclusions below that could aid future research by minimizing some often overlooked variables.

Main Conclusions

1. The Brown/Cook mechanical model theories were found not to hold for variable particle size with respect to MRR and resulting surface finish.
2. The chemical theory was supported by surface finish results from variable particle size and pH experiments, and MRR results from variable pH experiments.
3. The decrease in MRR with decreasing particle size is not fully understood with respect to the chemical model. The theoretical modeling planned for future work should provide insight into the number of available particles, loads on those particles and resulting contact area for chemical material removal.
4. The method of colloidal solution stability did not play a large role in MRR of silica polishing. Some question still exists as to why the polymeric coating on the non-ionic particle seemed to affect the overall surface finish of the workpiece.

Ancillary Conclusions

5. It was found that use of the overarm device on a traditional polishing system can drastically affect the pressure visible at the workpiece. A method was provided to overcome the condition by using constant weight load directly on the workpiece holder and removing the down force induced by the overarm quill.
6. A novel method for capturing MRR data was developed that eliminates any uncertainty involved with mass centric measurements (e.g. water adsorption, part cleanliness).

Future Work

As described in Chapter 6, the research performed answered some questions, but also raised others. Thus, there is a need for additional research to couple with the results presented in this thesis to answer some basic questions on the polishing process. The needed work is described below.

1. **Surface Chemistry Effects:** More information is needed on the effects of workpiece chemistry changes when in contact with varying pH solutions. An initial effort was attempted in this body of work, by measuring the Knoop hardness of silica materials exposed to solutions with pH 4-10. Unfortunately, no clear trend was evident, and it was assumed that the depth of the chemically affected layer must be much less than the depth of a micro-indent. However, out of this effort came the idea of performing scratch tests with varying pH abrasive slurries. This test would more directly describe the mechanical aspect of the polishing process.

2. Hydrodynamic Conditions During Polishing: Coupled with the scratch tests, determination of the frictional forces involved with polishing silica on pitch under varying pH conditions will be performed. It was noted during performance of this work that basic solutions were visibly ‘slicker’ than acidic solutions. These frictional force measurements could provide insight into whether there are regimes of hydrodynamic skating of the workpiece, so a test to determine the coefficient of friction at each pH level is warranted. The work will be accomplished using the deterministic polishing head currently under test in the Advanced Surfaces Group [57].

3. Theoretical Modeling: Applying existing theoretical models is also of interest to this body of work. An existing model has been proposed by researchers at Motorola [58], which describes a CMP model that accounts for roughness of the polishing pad. Although it is centered on CMP, the theory is modeled as a pad surface with bumps, much like the configuration of abrasive particles protruding from pitch. The modeling equations predict removal rates based not only on applied pressure, but also the pressure that is seen at the particle level. Application of these theories to pitch polishing could be developed, and experiments designed to compare with the analytical results by utilizing variables such as number of available particles, applied pressure, pressure at an individual particle and their effects on indentation depth and contact area.

Final Thoughts

The results provided in this thesis will hopefully serve as a starting point for future work on the subject with the Advanced Surfaces Group of the Center for Precision Metrology, UNC-Charlotte. Experimental validation has been provided that shows chemical tooth as the dominant removal mechanism in ceria-silica polishing. However, this work is merely a launching pad for additional experimentation that will continue the focus on basic science in polishing and the application of that science to a variety of glass.

The nature of polishing can be unpredictable. Even with strict control of process parameters, there is little certainty in predicting approximate removal rates and resulting surface finish. Work of this type will continue, drilling down on the more scientific aspects, versus just trying to reach the end goal. With better understanding of the underlying science of a particular polishing scheme, like the one presented here, transitions to different glass – particle – polisher configurations can be made that will hopefully reduce the expensive and time consuming process of polishing.

REFERENCES

1. Lu, P.J., Yao, N., So, J.F., Harlow, G.E., Lu, J.F., Wang, G.F., 2005, "The Earliest Use of Corundum and Diamond In Prehistoric China," *Acrhaeometry*, **47(1)**: 1-12.
2. Miniati, M., Van Helden, A., Greco, V., Molesini, G., 2002, "Seventeenth-Century Telescope Optics of Torricelli, Divini, and Campani," *App. Opt.*, **41(4)**: 644-647.
3. Gillman, B.E., Tinker, F., 1999, "Fun Facts About Pitch and the Pitfalls of Ignorance," *Proc. of SPIE*, **3782**: 72-79.
4. Preston, F.W., 1923, "On the Properties of Pitch Used in Working Optical Glass," *Trans. of Opt. Soc.*, **24(3)**: 117-142.
5. Brown, N.J., 1977, "Optical Polishing Pitch," LLNL Document UCRL-80301, Preprint for OSA Workshop on Optical Fabrication and Testing, San Mateo, CA, November 10th - 12th.
6. Gee, A., "Modelling the Mechanics of Free Particulate Abrasive Polishing from the Viewpoint of Single-Point Processes," *Proc. Of SPIE*, **2775**: 611-618.
7. Sutton, S.P., 2004, "Development of New Synthetic Optical Polishing Pitches," OSA Conference on Optical Fabrication and Testing, Paper OTuA2, Rochester, NY, October 10th.
8. Tesar, A.A., Fuchs, B.A., 1991, "Removal Rates of Fused Silica with Cerium Oxide/Pitch Polishing," *Proc. of SPIE*, **1531**: 80-90.
9. Murray, P.G., 2004, "Nanocrystalline Cerium Oxide Improves Glass Polishing Operations," *Photonics Spectra*, August Issue.
10. Nanophase Technologies Corporation, March 2005, Product Data Sheet, NanoTek[®] Cerium Oxide, CE-6082.
11. Nanophase Technologies Corporation, March 2005, Product Data Sheet, NanoTek[®] Cerium Oxide, CE-6086.
12. Murray, P.G., Personal Correspondence, 5 October 2006.
13. Izumitani, T.S., 1986, *Optical Glass*, English Translation from American Institute of Physics, New York, NY: 1-3.
14. Radel, S.R., Navidi, M.H., 1994, "Chemistry," West, St. Paul, MN: 562.

15. Roberts, W. L., Campbell, T. J., and Rapp Jr., G. R., 1990, Encyclopedia of Minerals, 2nd Ed., Van Nostrand Reinhold, New York: 709-710.
16. Hammond, C., 2001, "The Basics of Crystallography and Diffraction," 2nd Ed., Oxford Univ. Press, New York, NY: 89-92.
17. Sawyer Technical Materials LLC, September 1999, Hydrothermal Growth of Quartz. [online] http://www.sawyerresearch.com/Main_library.htm.
18. Shchipalov, Y.K., 2000, "Surface Energy of Crystalline and Vitreous Silica," Glass and Ceramics, **57(11-12)**: 374-377.
19. Saint-Gobain Quartz, April 2006, Saint-Gobain Quartz Optical Products and Materials, Technical Publication APR 06-GR-A4-EN. [online] <http://www.quartz.saint-gobain.com>.
20. Saint-Gobain Quartz, March 2006, Spectrosil® Optical Fused Silica, Technical Publication MAR 06-GR-A4-EN. [online] <http://www.quartz.saint-gobain.com>.
21. Sawyer Technical Materials, LLC, 'Good' Fundamental Material Constants for Crystalline Quartz, Technical Publication. [online] http://www.sawyerresearch.com/Main_library.htm.
22. Saint-Gobain Quartz, June 2005, Fused Quartz & Fused Silica, Material Properties Data Sheet, Technical Publication JUN 05-GR-A4-EN. [online] <http://www.quartz.saint-gobain.com>.
23. Levien, L., Prewitt, C. T., Weidner, D. J., 1980, "Structure and Elastic Properties of Quartz at Pressure," American Mineralogist, **65**: 920-930.
24. Schott North America, Inc., Product Information on Zerodur®. [online] http://www.us.schott.com/optics_devices/english/products/zerodur/index.html.
25. Evans, C.J., Paul, E., Dornfield, D., Lucca, D.A., Byrne, G., Tricard, M., Klocke, F., Dambon, O., Mullany, B.A., 2003, "Material Removal Mechanisms in Lapping and Polishing," Ann. of CIRP - Manuf. Tech., **52(2)**: 611-633.
26. Lord Rayleigh, 1917, "Polish," Trans. Opt. Soc., **19(1)**: 38-47.
27. Ref. [13]: 91-148.
28. Preston, F.W., 1926, "The Nature of the Polishing Operation," Trans. Opt. Soc., **27(3)**: 181-190.
29. Preston, F.W., 1927, "The Theory and Design of Plate Glass Polishing Machines," Soc. Glass Tech., **11**: 214-256.

30. Komanduri, R., Lucca, D.A., Tani, Y., 1997, "Technological Advances in Fine Abrasive Processes," *Ann. of CIRP*, **46(2)**: 545-596.
31. Brown, N., Baker, P., Maney, R., 1981, "Optical Polishing of Metals," *Proc. Of SPIE*, **306**: 42-57.
32. Brown, N.J., Fuchs, B.A., 1989, "Shear Mode Grinding," *IEEE Symp. on Freq. Control*: 606-610.
33. Brown, N.J., Cook, L.M., 1984, Paper TuB-A4, *Tech. Digest, Topical Meeting on the Science of Polishing*, OSA, 17 Apr. 1984.
34. Brown, N., 1986, "Preparation of Ultrasooth Surfaces," *Ann. Rev. Mater. Sci.*, **16**: 371-88.
35. Cook L.M., 1990, "Chemical Processes in Glass Polishing," *J. of Non-Cryst. Solids*, **120**: 152-171.
36. Tomozawa, M., Yang, K., Li, H., and Murarka, P., 1994, "Basic Science in Silica Glass Polishing," *Proc. Of Mat. Res. Soc. Symposia*, **337**: 89-98.
37. Osseo-Asare, K., 2002, "Surface Chemical Processes in Chemical Mechanical Polishing," *J. of Elec.-Chem. Society*, **149(12)**: G651-G655.
38. Paul, E., Personal Correspondence, 4-5 October 2006.
39. Ref. [14]: 752.
40. Malvern Instruments Ltd., *Zeta Potential, An Introduction in 30 Minutes*, Technical Note MRK654-01. [online] <http://www.malvern.com>.
41. Fuerstenau, D.W., Pradip, 2005, "Zeta Potentials in the Flotation of Oxide and Silicate Minerals," *Adv. Colloid Interface Sci*, **114-115**: 9-26.
42. Birdi, K.S., Ed., 1997, *Handbook of Surface and Colloid Chemistry*, CRC Press, Boca Raton, FL: 567.
43. Larson, R.G., 1999, *The Structure and Rheology of Complex Fluids*, Oxford University Press, NY: 326-329.
44. Hoshino, T., Kurata, Y., Terasaki, Y., Susa, K., 2001, "Mechanism of Polishing SiO₂ Films by CeO₂ Particles," *J. of Non-Cryst. Solids*, **283**: 129-136.
45. Abiade, J. T., and Choi, W., 2005, "Effect of pH on Ceria-Silica Interactions During Chemical Mechanical Polishing," *J. Mater. Res.*, **20(5)**: 1139-1145.

46. Suphantharida, P., and Osseo-Asare, K., 2004, "Cerium Oxide Slurries in CMP. Electrophoretic Mobility and Adsorption Investigations of Ceria/Silicate Interaction," *J. of Elec. Soc.*, **151 (10)**: G658-G662.
47. Cumbo, M.J., Fairhurst, S.D., Jacobs, S.D., and Puchebner, B.E., 1995, "Slurry Particle Size Evolution During the Polishing of Optical Glass," *App. Opt.*, **34(19)**: 3743-3755.
48. Tesar, A.A., Fuchs, B.A., Hed, P.P., 1992, "Examination of the Polished Surface Character of Fused Silica," *App. Opt.*, **31(34)**: 7164-7172.
49. Nanophase Technologies Corporation, CE-6082 Technical Bulletin, CE-6082 Ceria Dispersion for Glass Polishing Application.
50. Matweb Material Property Data, Properties of Lead. [online]
<http://www.matweb.com/search/SpecificMaterial.asp?bassnum=AMEPb00>.
51. Leistner, A.J., Thwaite, E.G., Lesh, F., Bennett, J.M., 1992, "Polishing Study Using Teflon and Pitch Laps to Produce Flat and Supersmooth Surfaces," *App. Opt.*, **31(10)**: 1472-1482.
52. Leistner, A.J., 1993, "Teflon Laps: Some New Developments and Results," *App. Opt.*, **32(19)**: 3416-3424.
53. National Institute of Standards and Technology, Roughness Parameters Technical Document, Internet Based Surface Metrology Algorithm Testing System. [online]
<http://ats.nist.gov/VSC/jsp/>.
54. Precision Devices, Inc., 1998, Surface Profile Parameters. [online]
<http://www.predev.com/smg/pdf/SurfaceRoughness.pdf>.
55. Iler, R., 1979, "The Chemistry of Silica," Wiley, New York, NY.
56. Paul, E., Personal Correspondence, 19 October 2006.
57. Mullany, B., Williams, W., 2006, "Real time measurement of Friction and Vibration during Polishing", Proceeding of the ASPE Annual Conference, Monterey, CA, October 16th - 19th.
58. Yu, T.K., Yu, C.C., Orłowski, M., 1993, "A Statistical Polishing Pad Model for Chemical-Mechanical Polishing," *Proc. of IEEE Int. Elect. Dev. Meeting*: 865-868.